Deuteron-induced reactions on ^{nat}Zr up to 60 MeV

E. Šimečková,[1,*] M. Avrigeanu,[2,†] J. Mrázek,[1] J. Novak,[1] M. Štefánik,[1] C. Costache,[2] and V. Avrigeanu[2]

[1]*Nuclear Physics Institute of the CAS, 25068 Řež, Czech Republic*

[2]*Horia Hulubei National Institute for Physics and Nuclear Engineering, P.O. Box MG-6, 077125 Bucharest-Magurele, Romania*

(Received 14 July 2021; revised 26 August 2021; accepted 5 October 2021; published 15 October 2021)

Background: The deuteron weak binding energy is responsible for high complexity of the deuteron interaction with nuclei that involves also a variety of reactions initiated by the nucleons following the deuteron breakup (BU). An update of both the scarce experimental deuteron database and the incomplete theoretical frame of the deuteron activation analysis is thus needed. Removal of discrepancies between experimental data, and a consistent inclusion of BU as well as of stripping and pickup direct reactions (DR) contributions within deuteron activation analysis, besides preequilibrium emission (PE) and fully equilibrated compound nucleus (CN) decay, are essential, too.

Purpose: Accurate new measurements of low-energy deuteron-induced reaction cross sections for natural Zr target are intended to enhance the related database and the opportunity for a unitary and consistent account of BU, DR, PE, and CN involved reaction mechanisms.

Methods: The activation cross sections of ^{90,91m,92m,94m,95m,95g,96,97}Nb, ^{89m,89,95,97}Zr, and ^{87m,87g,87,88,90m,91m,94}Y nuclei in deuteron-induced reactions on Zr at energies up to 20 MeV were measured by the stacked-foil technique and high-resolution γ spectrometry using the U-120M cyclotron of the Center of Accelerators and Nuclear Analytical Methods (CANAM) infrastructure of the Nuclear Physics Institute of the Czech Academy of Sciences (NPI CAS). Their extended analysis, together with all available data for deuteron interactions with Zr isotopes up to 60 MeV, has included every process from elastic scattering until CN evaporation, with particular attention paid to BU and DR mechanisms.

Results: Newly measured activation excitation functions proved essential for the deuteron database, while analysis of all available data strengthens their consistent account provided that (i) suitable BU and DR assessment is completed by (ii) PE and CN contributions corrected for total-reaction cross-section decrease due to the leakage of the initial deuteron flux towards BU and DR processes.

Conclusions: The suitable description of nuclear mechanisms involved within deuteron-induced reactions on Zr, especially the BU and DR processes, is validated by overall agreement of the calculated and measured cross sections including the new experimental data at low energies.

DOI: 10.1103/PhysRevC.104.044615

I. INTRODUCTION

The present analysis of deuteron-induced reactions on Zr and its stable isotopes continues to extend the database of deuteron data as well as consistent model accounts [1–9], requested by ongoing strategic research programs at large-scale facilities using deuteron beams [10–12]. Actually, the deuteron weak binding energy $B_d = 2.224$ MeV is responsible for high complexity of the deuteron interaction that involves also a variety of reactions induced by the nucleons following the deuteron breakup (BU) [1,3,5,9,13–15]. The need to update both the scarce experimental database and the incomplete theoretical frame of the deuteron activation analysis within, e.g., the FENDL library [16] concerns also natural zirconium, which is a constituent of CuCrZr alloys, candidate material for ITER [10] and DEMO [17] structures. Thus, being aware of the discrepancies between measured data, the consistent inclusion of the BU contribution as well as of stripping (d, p) and (d, n) and pickup (d, t) and (d, α) direct reactions (DR) within deuteron activation analysis becomes feasible, too, in addition to handy recommended Padé fits [18,19].

Consequently, this work aims both to strengthen the database of deuteron-induced reactions on Zr, up to 20 MeV, and achieve a deeper understanding of deuteron BU and poorly taken into account DR, besides the well-established preequilibrium (PE) and emission from the fully equilibrated compound nucleus (CN). Consistent model calculations have been involved in this respect, namely (i) by using the same parameters of, e.g., optical potentials, in the framework of BU, DR, PE, and CN models, and (ii) looking for a suitable description of all available data for competitive reaction channels, in order to avoid less accurate parameter-error compensation effects.

The present-work experimental setup and the measured data are described in Sec. II. Then, a consistent energy-

*simeckova@ujf.cas.cz

†marilena.avrigeanu@nipne.ro

dependent optical potential for deuterons on Zr isotopes is discussed in Sec. III A. The theoretical framework of the deuteron BU mechanism is the subject of Sec. III B, while the DR analysis using the computer code FRESCO [20] is described in Sec. III C. Contributions of the within TALYS-1.95 code [21] are described in Sec. III D. The measured and calculated deuteron activation cross sections of natural Zr and its stable isotopes are compared in Sec. IV, including the evaluated data from the TENDL-2019 library [22], while conclusions are given in Sec. V.

II. MEASUREMENTS

The irradiation was carried out on the Center of Accelerators and Nuclear Analytical Methods (CANAM) infrastructure of the Nuclear Physics Institute of the Czech Academy of Sciences (NPI CAS) using an external deuteron beam of the variable-energy cyclotron U120-M operating in the negative-ion mode. The beam was extracted using a stripping-foil extractor and was delivered to the reaction chamber through a beam line consisting of one dipole and two quadrupole magnets. The mean beam energy was determined with an accuracy of 1%, with FWHM of 1.8%.

The activation cross sections were measured by a stacked-foil technique. The collimated deuteron beam of 20.02 MeV energy struck the stack of foils in a Faraday-cup-like chamber. This setup enables the cooling of the stacked foils without the loss of accuracy in the beam and charge monitoring. Stacked foils were irradiated by a 0.33 μA deuteron beam during 620 s (total charge 203.5 μC).

The high purity metallic Zr foils (99.9%, 25 μm, Goodfellow product) were interleaved by Al foils (99.9%, 50 μm, Goodfellow product) serving as an additional monitor and for energy reduction. The foils were weighed to avoid relatively large uncertainties in foil thicknesses declared by the producer. The mean energy, energy thickness, and energy straggling in each foil were calculated by SRIM 2008 code [23]. Natural zirconium consists of five stable isotopes: ^{90}Zr (51.45%), ^{91}Zr (11.22%), ^{92}Zr (17.15%), ^{94}Zr (17.38%), and ^{96}Zr (2.80%).

The γ rays from the irradiated foils were measured repeatedly by two calibrated high-purity germanium (HPGe) detectors of 50% efficiency. The measurements at different cooling times lasted ≈50 days after irradiation. Activated isotopes were identified on the basis of $T_{1/2}$, γ-ray energies, and their intensities [24] given in Table I.

Experimental errors consist of statistical errors of γ-peak counting, systematic errors of the charge measurement (5%), uncertainty of foil thicknesses (2%), and detector efficiency uncertainty (2%).

The measured cross sections of the ^{97}Nb, ^{96}Nb, ^{95}Nb^m, ^{95}Nb^g, ^{94}Nb^m, ^{92}Nb^m, ^{91}Nb^m, ^{90}Nb^{m+g}, ^{97}Zr, ^{95}Zr, ^{89}Zr^m, ^{89}Zr, ^{94}Y, ^{91}Y^m, ^{90}Y^m, ^{88}Y, ^{87}Y, ^{87}Y^m, ^{87}Y^g activation through $^{\text{nat}}$Zr(d,x) reactions at energies between 4 and 20 MeV are shown in Tables II and III. The detailed analysis of each measured excitation function and comparison with recent data [25–28] are given in Sec. IV, while comments on peculiarities of several residual-nuclei's activation are given thereafter.

TABLE I. Half-lives, main γ lines, and their intensities [24] of the isotopes observed from irradiated Zr foils. The transitions marked by a star were used in the analysis.

Isotope	$T_{1/2}$	E_γ (keV)	I_γ (%)	
^{97}Zr	16.91 h	743.36	93	
^{97}Nb	72.1 min	658.08	98	*
^{96}Nb	23.35 h	778.22	96.45	
		568.8	58	
		495.88	26.62	
^{95}Zr	64.02 h	756.73	54	
		724.20	44.17	
^{95}Nb^m	86.6 h	235.69	24.5	*
^{95}Nb^g	34.975 d	765.8	100	*
^{94}Y	18.7 min	918.74	56	
^{94}Nb^m	6.263 min	871.09	0.50	
^{92}Nb^m	10.15 d	934.46	99	
^{91}Y^m	49.71 min	555.57	95	
^{91}Nb^m	60.86 d	1204.77	2.9	
		104.62	0.539	
^{90}Nb	14.6 h	1129.22	92.7	
		2318.97	82.03	
		141.18	66.8	
^{90}Y^m	3.19 h	202.51	97.3	
		479.17	90.74	
^{89}Zr^m	4.18 min	587.83	90	
^{89}Zr	78.41 h	908.96	100	
		1713.06	0.763	
^{88}Y	106.65 d	1836.06	99.2	
		898.04	93.7	
^{87}Y^m	13.37 h	380.79	78	
^{87}Y^g	79.8 h	484.81	89.7	*
^{87}Y	79.8 h	484.81	89.7	
		388.53	82	

The activation cross sections of the ^{97}Nb residual nucleus were determined from analysis of the time dependence of the 658.08 keV activity using Bateman formula, as there are two contributions to it, the second originating from the decay of the ^{97}Zr residual nucleus. The activity of ^{97}Zr at the end of the irradiation was determined independently and was used as a fixed parameter.

The situation is similar for ^{95}Nb^m (235.69 keV level, 3.61 d) produced in the (d,x) reaction, which decays solely to the ground state (g.s.). This 235.69 keV level is also populated by decay of ^{95}Zr, being fed by 1.08% of the total activity [29]. The independently determined activity of ^{95}Zr at the end of the irradiation and the above branching parameter were fixed for the fit.

In the case of ^{95}Nb^g, the contributions from the (d,x) reactions and from the progenitors (^{95}Nb^m 1.08%, ^{95}Zr 98.9%) were disentangled by the analysis of the 765.8 keV line (belonging to ^{95}Mo) time evolution (six different points from a few to 1000 hours after the irradiation). Similarly to the previous case, we have used the independently determined activity of ^{95}Zr and ^{95}Nb^m in the fit. We have also set free all the three parameters to estimate the consistency of the method; the difference of ^{95}Nb^g calculated activity in this case

TABLE II. Measured Nb and Zr ($A > 90$) residual-nuclei activation cross sections (mb) for deuterons incident on natural zirconium. The displayed energy uncertainty is a combination of the energy thickness of each foil and the initial-energy spread. The uncertainties are given in parentheses, in units of the last digit.

Energy (MeV)	^{97}Nb	^{96}Nb	^{95}Nb^{m}	^{95}Nb^{g}	^{94}Nb^{m}	^{92}Nb^{m}	^{91}Nb^{m}	^{90}Nb	^{97}Zr	^{95}Zr
4.32(60)	0.29(6)	0.19(1)	0.98(11)	1.45(16)		1.18(7)	3.29(31)	0.10(1)	0.32(2)	3.29(13)
6.54(46)	2.00(41)	6.03(35)	8.13(92)	14.0(16)	22.0(28)	19.1(11)	45.8(33)	0.13(1)	4.03(23)	26.8(15)
8.33(40)	2.63(54)	16.04(93)	7.83(89)	15.7(18)	72.2(48)	60.4(36)	74.8(49)	0.17(1)	6.34(37)	42.9(25)
9.89(36)	2.04(42)	21.8(13)	6.77(77)	13.0(15)	98.8(84)	86.9)51)	74.2(47)	6.34(37)	5.91(35)	43.8(25)
11.29(33)	1.99(41)	24.7(14)	5.37(61)	11.6(13)	112(12)	96.3(62)	65.1(45)	100.6(58)	5.40(31)	40.0(23)
12.57(30)	1.72(36)	24.5(14)	6.17(70)	14.4(16)	111(14)	110.2(66)	55.3(33)	216.(13)	4.81(28)	37.9(22)
13.77(29)	1.29(27)	21.2(12)	6.94(79)	17.3(20)	103(29)	104.3(62)	44.9(32)	311.(18)	4.31(27)	33.3(19)
14.89(27)	0.89(18)	17.1(10)	7.03(80)	23.6(27)	73(10)	105.6(62)	44.6(28)	359.(21)	3.83(25)	31.2(18)
15.96(26)	1.33(28)	13.91(81)	7.37(84)	28.0(32)	60.7(93)	86.2(50)	40.3(24)	395.(23)	3.51(21)	28.4(16)
16.98(25)	0.96(20)	11.37(67)	7.81(89)	29.6(34)		76.4(46)	40.6(29)	404.(24)	3.26(22)	26.0(15)
17.95(24)	1.19(25)	9.91(58)	7.87(89)	32.4(37)	38.6(40)	62.1(36)	42.3(27)	432.(25)	3.11(22)	24.8(14)
18.89(23)	0.94(19)	8.50(50)	7.37(84)	34.5(39)		55.1(32)	42.3(26)	443.(26)	2.69(17)	23.1(13)
19.80(23)	0.91(19)	6.95(41)	7.52(85)	34.7(39)		44.6(26)	41.8(26)	452.(27)	2.52(17)	21.8(13)

was in the range of 10%. However, our results for ^{95}Nb^{g} differ from those of Tarkanyi *et al.* [26] by a factor 2 at around 10 MeV, the region of the maximum production cross section for ^{95}Zr. Since we did not find in [26] any information on the treatment of the feeding from ^{95}Zr (while the feeding from ^{95}Nb^{m} is discussed there), we tend to ascribe this difference to a neglected feeding from ^{95}Zr.

The activity of ^{91}Nb^{m} (60.86 d) was evaluated from the analysis of the γ line with energy 1204.77 keV (belonging to ^{91}Mo). It is populated in 2.8% of the decays. The same transition is populated in ^{91}Y (58.51 d) decay, with 0.3% intensity. The expected maximum cross section for ^{91}Y around 20 MeV is, however, two orders of magnitude lower than for ^{91}Nb^{m}. We did not observe any effect of the ^{91}Y decay in the 1204.77 keV transition, which is consistent with the mentioned low cross section.

The activation cross sections of $^{\text{nat}}$Zr$(d,x)^{87}$Y^{m} (13.37 h) were determined from the γ line 380.8 keV. This isomer decays to the g.s. (79.8 h), so the activation cross sections for $^{\text{nat}}$Zr$(d,x)^{87}$Y^{g} (with the 484.8 keV γ-line) were analyzed using the Bateman formula, as in the above cases. Moreover, the cumulative cross section for ^{87}Y^{g+m} was measured after 140 hours, when the feeding from ^{87}Y^{m} is already negligible.

III. NUCLEAR MODEL ANALYSIS

A. Optical potential assessment

A consistent input of nuclear model calculations should be proved [1–9] by the simultaneous analysis of the deuteron elastic scattering and induced activation, the optical model potential (OMP) parameters that are obtained by the former data fit being then used for calculation of all deuteron reaction cross sections. The Daehnick *et al.* [30] OMP was the first option of the present analysis, being obtained by use of a large experimental basis including also angular distributions of elastic scattered deuterons on $^{90-92,94,96}$Zr isotopes. It has been endorsed, too, by the present comparison of the experimental elastic-scattering angular distributions of deuterons on $^{90-92,94,96}$Zr [31–40] at incident energies between ≈5 and 56 MeV, and the calculated values using the computer code SCAT2 [41] and this OMP (Fig. 1). The good description of the measured data thus provided confidence for the

TABLE III. As in Table II but for Zr ($A < 90$) and Y isotopes activation.

Energy (MeV)	^{89}Zr^{m}	^{89}Zr	^{94}Y	^{91}Y^{m}	^{90}Y^{m}	^{88}Y	^{87}Y^{m}	^{87}Y^{g}	^{87}Y
4.32(60)			0.002(1)		0.004(1)	0.07(3)			
6.54(46)			0.036(4)		0.030(2)	0.45(4)			
8.33(40)			0.113(8)	0.006(1)	0.131(8)	1.76(11)			
9.89(36)		0.22(1)	0.139(14)	0.052(6)	0.259(15)	3.72(24)			
11.29(33)		0.45(7)	0.189(39)	0.147(15)	0.334(26)	5.83(38)			
12.57(30)		1.26(12)	0.202(30)	0.351(41)	0.397(33)	8.63(55)			0.06(1)
13.77(29)		2.34(18)	0.168(60)	0.559(53)	0.424(43)	9.59(56)	0.16(6)	0.23(3)	0.44(3)
14.89(27)	1.07(11)	3.38(20)		0.800(61)	0.409(41)	11.65(89)	0.83(17)	0.61(7)	1.62(9)
15.96(26)	1.47(13)	4.21(26)		1.012(64)	0.391(38)	12.14(77)	1.92(12)	1.32(15)	3.90(23)
16.98(25)		4.91(29)		1.290(86)	0.403(79)	11.80(76)	3.31(24)	2.60(29)	6.66(39)
17.95(24)	2.14(13)	6.41(37)	0.165(24)	1.60(12)	0.544(49)	11.78(74)	5.08(32)	3.92(45)	10 27(59)
18.89(23)	2.79(17)	11.17(65)	0.178(35)	1.78(11)	0.626(45)	11.52(74)	6.79(42)	4.98(57)	13.11(75)
19.80(23)	4.9(14)	21.3(13)		1.81(16)	0.780(65)	11.19(75)	8.41(51)	5.91(67)	15.99(93)

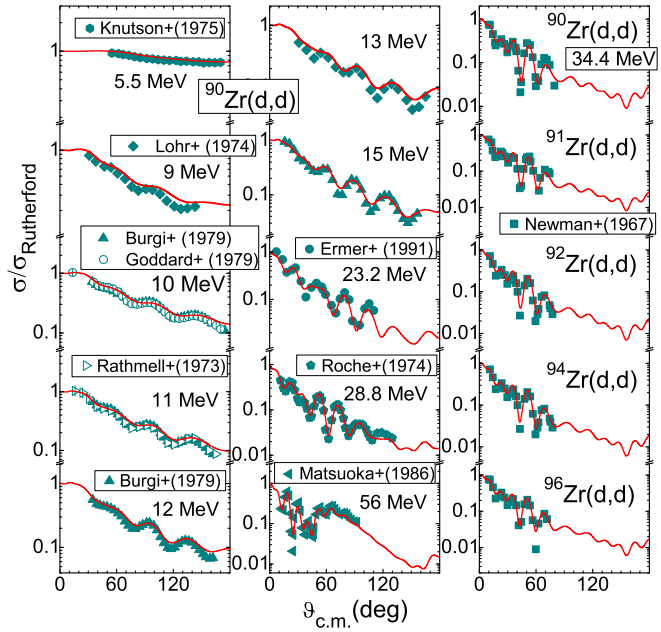

FIG. 1. Comparison of measured [31–40] and calculated elastic-scattering angular distributions of deuterons on ^{90,91,92,94,96}Zr at energies from ≈5 to 56 MeV, using the global OMP of Daehnick *et al.* [30].

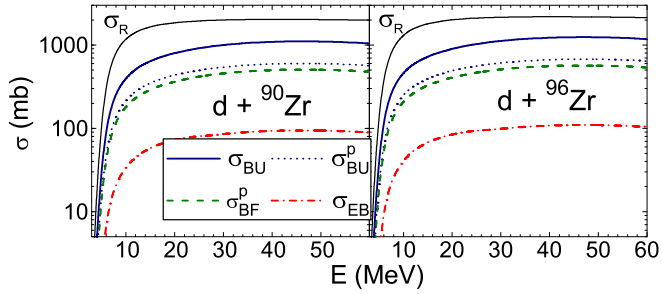

FIG. 2. The energy dependence of the deuteron total-reaction cross sections [30] (thin solid curves), total BU cross sections σ_{BU} (thick solid), and total BU proton-emission σ^p_{BU} (short-dashed), BF (dashed), and EB (dash-dotted) cross sections [15], for deuteron interactions with ^{90,96}Zr isotopes.

further use of this deuteron potential in calculation of the activation cross sections of the deuteron interaction with Zr isotopes.

The same deuteron OMP as well as the nucleon, triton, and α-particle OMPs (Sec. III D) were then incuded within each of the BU, DR, PE, and CN models, for a consistent model analysis.

B. Deuteron breakup

Details concerning the physical picture of the deuteron breakup in the Coulomb and nuclear fields of the target nucleus were given recently [7,9,15]. Therefore, only particular points are mentioned hereafter for the distinct processes that are considered in this respect, namely the elastic breakup (EB) in which the target nucleus remains in its ground state and none of the deuteron constituents interacts with it, and the inelastic breakup or breakup fusion (BF), where one of these deuteron constituents interacts nonelastically with the target nucleus.

The parametrization [15] of both EB cross section σ_{EB} and total BU proton-emission cross section $\sigma^p_{BU} = \sigma_{EB} + \sigma^p_{BF}$ was obtained through analysis of the experimental systematics of deuteron-induced reactions on target nuclei from ^{27}Al to ^{232}Th [42–46]. Equal BF nucleon-emission cross sections σ^n_{BF} and σ^p_{BF} were assumed [46], so that the total BU cross section is $\sigma_{BU} = \sigma_{EB} + 2\sigma^{n/p}_{BF}$ Actually, the ratios of σ^p_{BU} and σ_{EB} to the deuteron total-reaction cross section σ_R were parametrized, i.e., $f^{n/p}_{BU} = \sigma^{n/p}_{BU}/\sigma_R$ and $f_{EB} = \sigma_{EB}/\sigma_R$, respectively. Their dependence on deuteron incident energy E, as well as target-nucleus atomic Z and mass A numbers, is given by

$$f^{n/p}_{BU} = 0.087 - 0.0066Z + 0.00163ZA^{1/3} + 0.0017A^{1/3}E - 0.000002ZE^2, \quad (1)$$

$$f_{EB} = 0.031 - 0.0028Z + 0.00051ZA^{1/3} + 0.0005A^{1/3}E - 0.000001ZE^2, \quad (2)$$

while more details concerning the extrapolation of f_{EB} beyond the energy domain of experimental systematics, and the constraint due to scarce data exiting for heaviest target nuclei ($A > 200$), are given elsewhere [14,15]. The energy dependence of σ_R, σ_{BU}, σ^p_{BU} as well as of the components σ_{EB} and σ^p_{BF} is shown in Fig 2 for deuteron interactions with ^{90,96}Zr isotopes. The BU excitation functions increase with increasing deuteron-energy, while their dominant BF component is quite important for the analysis of two opposite BU effects on deuteron-activation cross sections, briefly recalled later.

First, the total-reaction cross section that is shared among different outgoing channels is reduced by the value of σ_{BU}. On the other hand, the BF component brings additional contributions to different reaction channels [1–9,47–49]. Then, interactions of the BF proton or neutron with the target nucleus contribute to enhancement of the corresponding (d, xn) or (d, xp) reaction cross sections, respectively. The compound nuclei in reactions induced by the BF nucleons differ by one unit of A and maybe also of Z than in deuteron-induced reactions. The partition of the BF cross section among various residual-nuclei population is triggered by the energy spectra of the BF nucleons and the excitation functions of the reactions induced by these nucleons on the target nuclei [9,49].

Interpolation of nucleon-induced reaction cross sections available either experimentally [40] or evaluated [22] has been used in estimation of the nucleon-enhancing ratios [9,49], in order to reduce as much as possible the supplementary uncertainties brought by additional theoretical calculations.

Lastly, the BF enhancements by the BU nucleons corresponding to deuterons incident on ^{nat}Zr, through (n, γ), $(n, 2n)$, (n, xp), $(n, xnyp)$, (p, γ), (p, xn), $(p, 2p)$, and $(p, xnyp)$ reactions, are discussed in Sec. IV (Figs. 10–23).

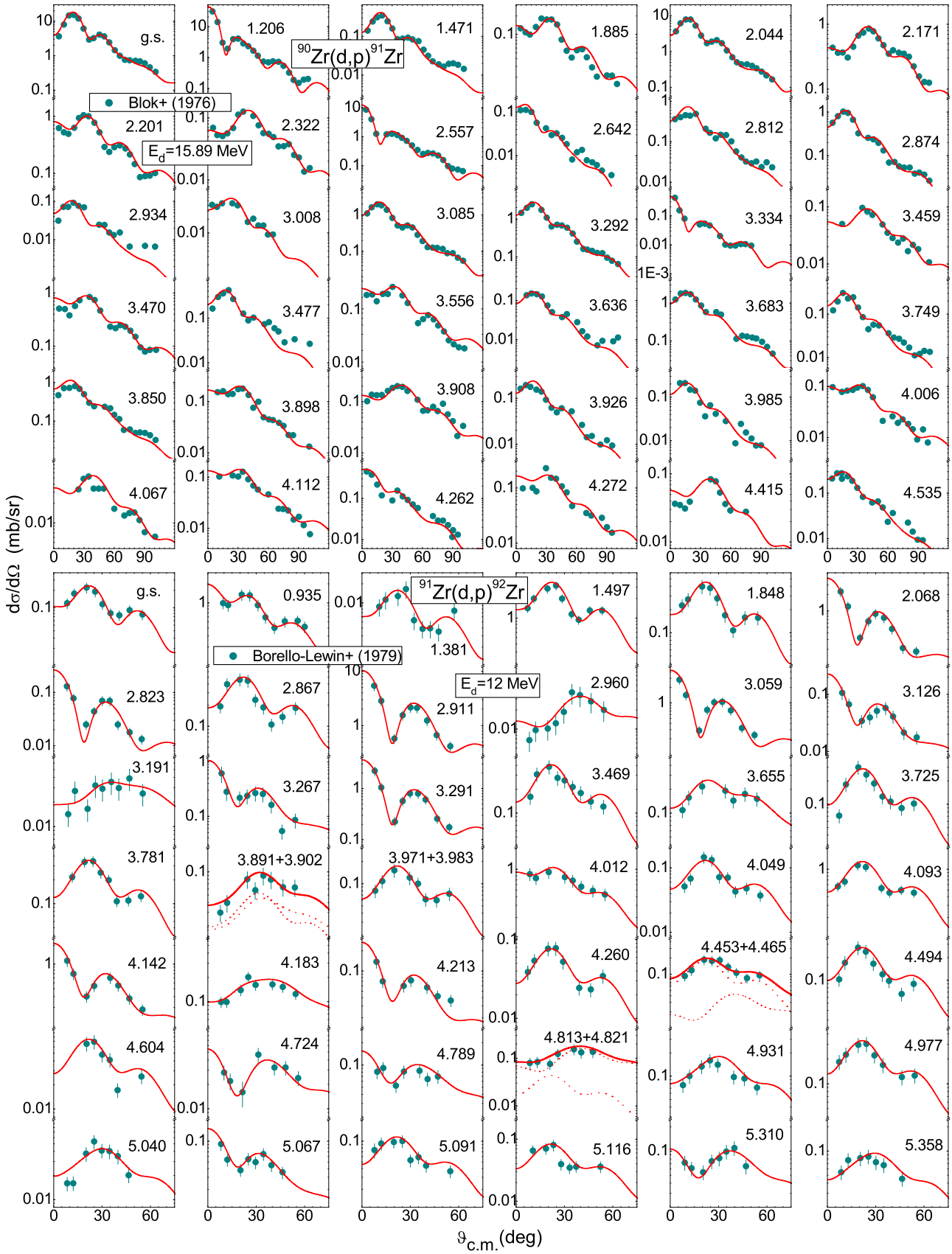

FIG. 3. Comparison of measured [62,63] and calculated (solid curves) proton angular distributions of ^{90}Zr$(d, p)^{91}$Zr (top) and ^{91}Zr$(d, p)^{92}$Zr (bottom) stripping transitions to states with excitation energies in MeV, at incident energies of 15.89 and 12 MeV, respectively.

C. Direct reactions

The DR mechanism [49] remains quite important for estimation of the of first-chance emitted particle (d, p), (d, n), (d, t), and (d, α) reaction cross sections, especially around the Coulomb barrier. Poor attention given so far to this issue may account for the problems noted even nowadays with respect to the theoretical modeling of deuteron-induced reactions [18,19,50].

On the other hand, the (d, p) stripping reaction has particularly been of major importance for nuclear structure studies, with the spectroscopic factors extracted from proton angular-distributions analysis contributing to validation of the nuclear shell model. Consequently, the rich systematics of transferred proton angular distributions made possible in the present work the detailed analyses of the (d, p) stripping process on ^{90,91,92,94,96}Zr isotopes.

The appropriate calculation of the DR stripping and pickup mechanisms' contributions in this work used the distorted-wave Born approximation (DWBA) formalism within the code FRESCO [20]. The post/prior form distorted-wave transition amplitudes for $(d, n/p)$ stripping and respectively $(d, t/\alpha)$ pickup reactions, and the finite-range interaction, have been considered. The n-p effective interaction in deuterons [51] as well as the d-n effective interaction in tritons [52] were assumed to have a Gaussian shape, at the same time a Woods-Saxon shape [53] was assumed for the d-d

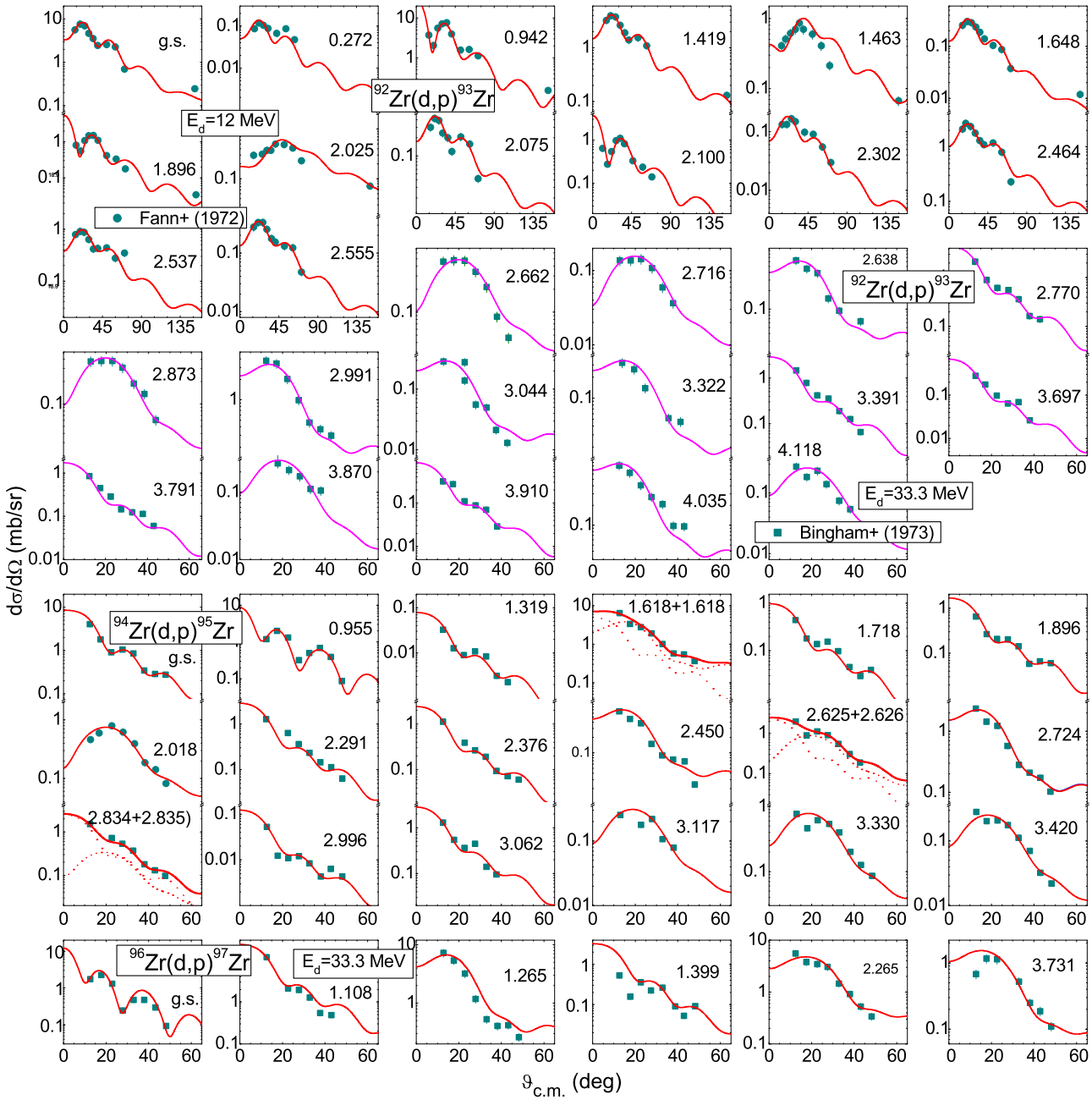

FIG. 4. As in Fig. 3 but for ^{92}Zr at 12 MeV [64] (top), ^{94}Zr (middle), and ^{96}Zr (bottom) at 33.3 MeV [65].

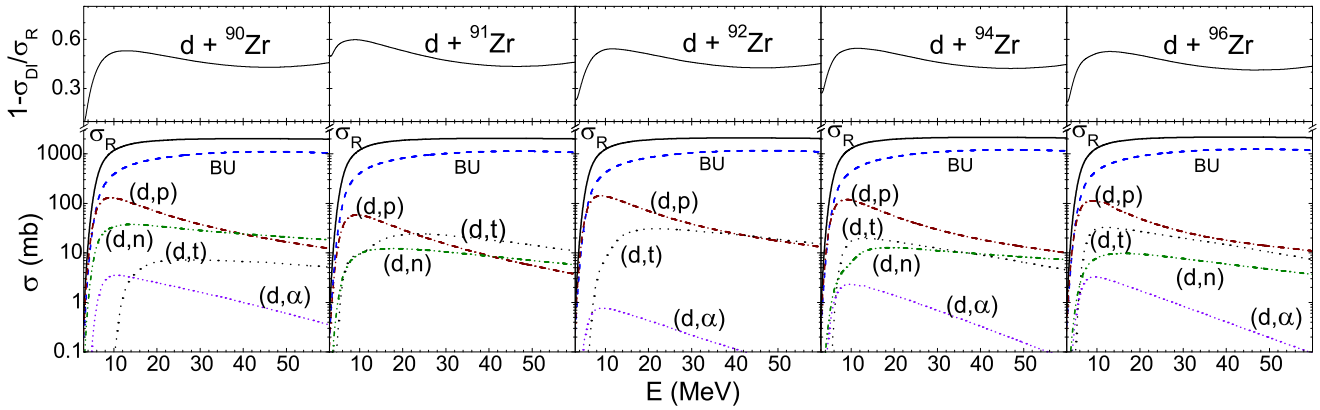

FIG. 5. Bottom: Energy dependence of the total-reaction (solid curves), total-breakup (dashed), as well as stripping (d, p) (dash-dotted) and (d, n) (dash-dot-dotted), and pickup (d, t) (dotted) and (d, α) (short-dotted) reaction cross sections of deuterons on $^{90–92,94,96}$Zr. Top: The corresponding reduction factors of the deuteron flux going towards PE + CN emission.

effective interaction in the α particle. The transferred nucleon and deuteron bound states were generated in a Woods-Saxon real potential [2,4–9,13]. The populated discrete levels and the corresponding spectroscopic factors available within the ENSDF library [54] were used as starting input of the DWBA calculations for the stripping and pickup reactions [55–61].

The analysis of the extensive protons angular distributions from $^{90–92,94,96}$Zr$(d, p)^{91–93,95,97}$Zr stripping reactions (Figs. 3 and 4) has provided the ultimate spectroscopic factors for transitions to discrete levels of residual nuclei, and the related calculated stripping cross sections. Thus, the numbers of residual-nuclei discrete levels considered in this respect were 51 in ^{91}Zr [54,55], 59 in ^{92}Zr [54,55], 39 in ^{93}Zr [54,55], 31 in ^{95}Zr [54,56], and 13 in ^{97}Zr [54,57]. Then, the suitable description of the available (d, p) angular distributions shown in these figures gives confidence in the corresponding theoretical stripping excitation functions shown at the bottom of Fig. 5.

Unfortunately, spectroscopic information corresponding to stripping (d, n) and pickup (d, t) and (d, α) reactions is available only for the most abundant isotope ^{90}Zr at a comparable level to that of the stripping (d, p) reaction. Thus, a suitable description of the angular distributions for these reactions [66–68] (Fig. 6) has validated the corresponding (d, n), (d, t), and (d, α) excitation function calculations also shown in Fig. 5 for this nucleus.

On the other hand, analysis of the only selected experimental triton angular distributions corresponding to the ground states of ^{90,91,93,95}Zr residual nuclei [69] (Fig. 7), at the same time with the use of spectroscopic factors provided by Refs. [54–56,58] for the rest of the pickup transitions, was involved in the calculation of the excitation functions of (d, t) pickup reactions on ^{91,92,94,96}Zr (also in Fig. 5).

Similarly, the analyses of selected experimental α-particle angular distributions [70,71] (Fig. 8) and spectroscopic factors provided by Refs. [54,55,58,59] have been considered for calculation of the pickup reaction ^{92,94,96}Zr$(d, \alpha)^{90,92,94}$Y excitation functions (Fig. 5).

We particularly comment on missing spectroscopic information for ^{91,94}Zr$(d, n)^{92,95}$Nb stripping reactions, needed to estimate the DR contribution to activation of the corresponding residual nuclei (Sec. IV). In this respect, we have adopted the spectroscopic factors of stripped proton by analysis of ^{91,94}Zr(^{3}He, d) stripping reactions [54,56,72], completed by analysis of available deuteron angular distributions from ^{91}Zr(^{3}He, d)^{92}Nb measured at 25.5 incident energy by Decman and Sheline [73] (Fig. 9). The d-p effective interaction in ^{3}He was assumed to have a Gaussian shape [74], similarly to (d, p) stripping analysis, while the transferred-proton bound states were generated in a Woods-Saxon real potential.

The spectroscopic factors S obtained in the present work by analysis of the experimental outgoing-particle angular distributions shown in Figs. 3, 4, and 6–9 are given in the Supplemental Material [75]. Their uncertainties, of obvious interest for detailed description of single-particle and collective features of even stable nuclei, exceeded the aim of the present DR account in completion of the deuteron activation of residual nuclei. Actually there were unquoted uncertainties on the above-mentioned S values [54–56,58,59] also used within this work, while significant changes of the spectroscopic factors extracted using DWBA may exist due to ambiguities in the optical and bound-state potentials (e.g., [76–78] and Refs. therein), and even the choice of the angular range where the fit is performed [79]. This is why, by using advanced global potentials, the finite-range DWBA method within the code FRESCO, and the enlarged angular range of the fitted data (Figs. 3, 4, 6–9), we expect the uncertainties of the present S values [75] are yet in the limit of 40% [78].

Concluding the suitable account of proton, neutron, deuteron, triton, and α-emission angular distributions of stripping (d, p), (d, n), (^{3}He, d), and pickup (d, t), (d, α) reactions on $^{90–92,94,96}$Zr (Figs. 3, 4, 6–9), reliable DR as well as BU contributions are summarized in Fig. 5. An overview of the deuteron flux, which, subsequently to these direct interactions (DI) processes, remains available for PE and fully equilibrated CN decay, is given by the σ_R reduction factor

$$1 - \frac{\sigma_{BU} + \sigma_{(d,n)} + \sigma_{(d,p)} + \sigma_{(d,t)} + \sigma_{(d,\alpha)}}{\sigma_R} = 1 - \frac{\sigma_{DI}}{\sigma_R}, \quad (3)$$

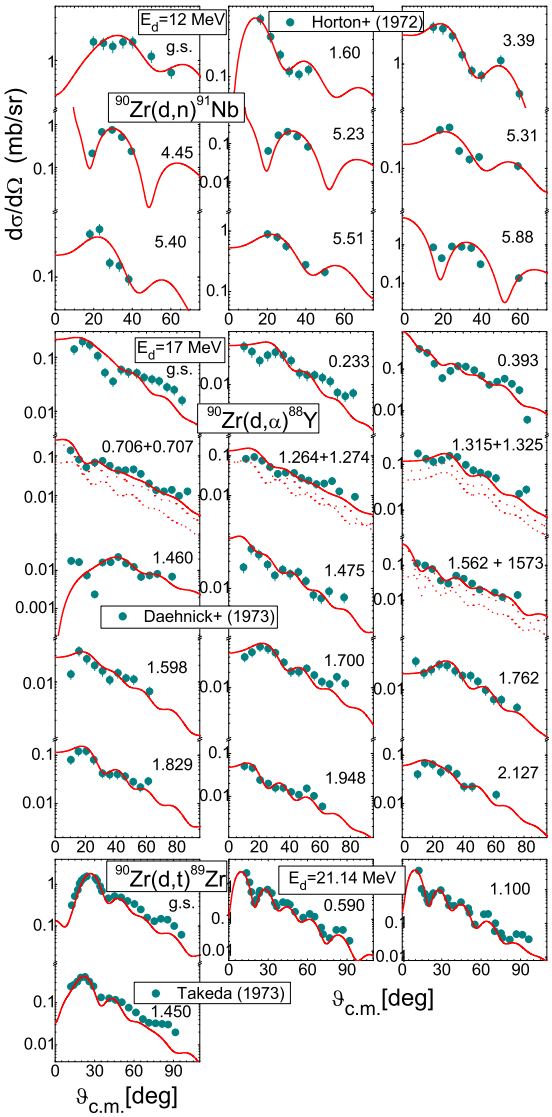

FIG. 6. As in Fig. 3 but for ^{90}Zr and (top) (d, n) stripping reaction at 12 MeV [66], (middle) (d, α), and (bottom) (d, t) pickup reactions at 17 MeV [67] and 21.14 MeV [68], respectively.

shown for $^{90-92,94,96}$Zr isotopes in Fig. 5 at once with the BU and DR excitation functions. Among the direct reactions considered in the present analysis there is obvious dominance of the (d, p) stripping process. Moreover, one may note first a steep increases with energy of the reduction factor since the major BU as well as the DR components increase with energy. The maximum of the (d, p) and (d, n) stripping excitation functions around 7–11 MeV is particularly obvious, providing the fastest slope of this factor. Then, the reduction factor reaches its own maximum and a slow decrease follows for all Zr isotopes due to an increase with energy of the BU + DR excitation functions that is slower than for σ_R. Thus, the remaining deuteron σ_R for the PE + CN statistical processes is slightly increasing above the deuteron energies of 15–20 MeV but close to only half of the OMP values. The important role of the direct interactions is thus pointed out.

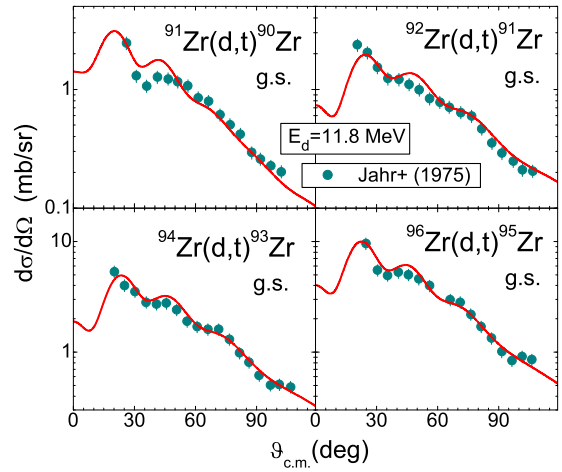

FIG. 7. As in Fig. 3 but for ^{91,92,94,96}Zr$(d, t)^{90,91,93,95}$Zr pickup transitions to the ground state of ^{90,91,93,95}Zr residual nuclei, at 11.8 MeV [69].

D. Statistical emission

The PE and CN statistical processes become important with the incident-energy increase (e.g., [49]). The corresponding reaction cross sections and additionally the inelastic breakup enhancement [5–9,47,48] have been calculated using the TALYS-1.95 code [21]. The above-mentioned deuteron-flux absorption into the DR processes has been taken into account, too.

The following input options of the TALYS code have been used: (a) the OMPs of Koning-Delaroche [80], Daehnick *et al.* [30], Becchetti-Greenlees [81], and Avrigeanu *et al.* [82] for neutrons and protons, deuterons, tritons, and α particles, respectively, (b) the back-shifted Fermi gas (BSFG) formula for the nuclear level density [83,84] including the damping of shell effects with excitation energy in single-particle level densities, and (c) analytical PE transition rates with energy-dependent matrix element. The breakup model 2 option has been also used for deuteron breakup cross section calculations, including the inelastic breakup enhancement [6,15].

Actually, the PE and CN mechanisms' contribution shares around half of the deuteron total-reaction cross section σ_R, as shown in Fig. 5. It is discussed in the following for each residual nucleus activation, in comparison to the breakup and direct reactions ones.

IV. RESULTS AND DISCUSSION

The excitation functions of particular residual nuclei resulting from deuteron interaction with ^{nat}Zr, measured in the present work (Sec. II), are compared with the formerly available data [40], the corresponding TENDL-2019 evaluation [22], and the results of calculations using FRESCO [20] and TALYS [21] codes. The measured excitation functions for the population of ^{97}Nb, ^{94}Nb^m, ^{89}Zr^m, ^{94}Y, and ^{91}Y^m residual nuclei are for the first time reported in the present work, while the rest of measured cross sections are in particularly good agreement with the more recent data [25–28].

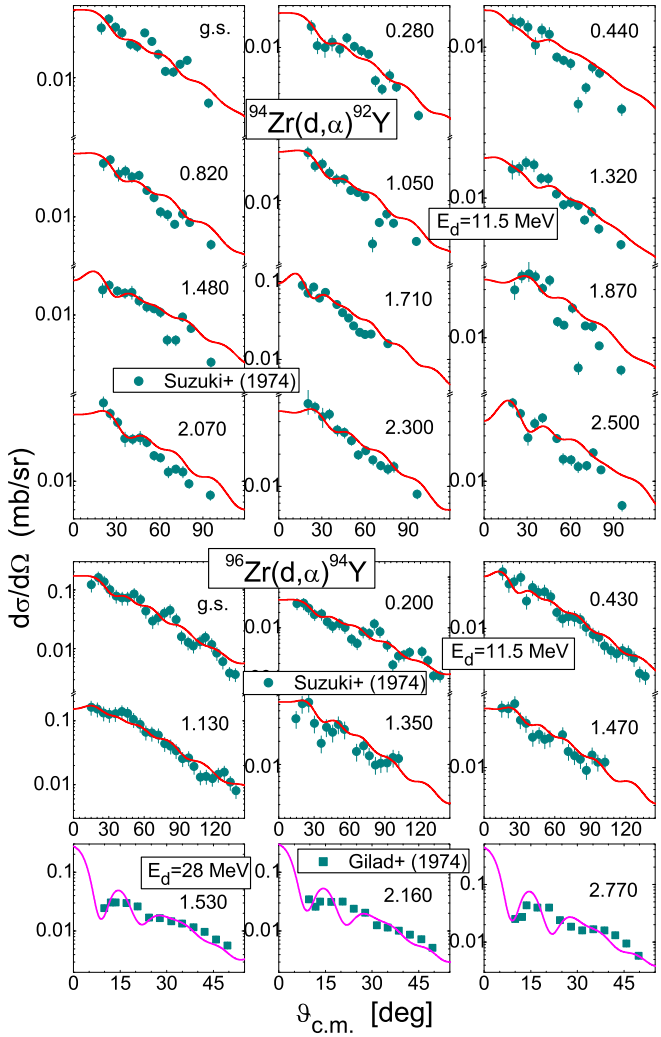

FIG. 8. As in Fig. 3 but for (top and middle) ^{94,96}Zr$(d,\alpha)^{92,94}$Y pickup reactions at 11.5 MeV [70] and (bottom) 28 MeV [71].

The detailed contributions of various reaction mechanisms, pointing out the strength of each one, and of the Zr isotopes to the activation of a certain residual nucleus are presented following three residual nuclei sequences: ^{nat}Zr$(d,xn)^{97-90}$Nb (Figs. 10–15), ^{nat}Zr$(d,xnp)^{97-88}$Zr (Figs. 16–19), and ^{nat}Zr$(d,xn2p)^{91-86}$Y (Figs. 20–23). While some negligible contributions to the activation of particular residual nuclei are not shown for specific Zr stable isotopes in Figs. 10–23, they were all considered within the cross-section calculation for natural Zr target.

The proper description of the reaction mechanisms considered in this work is proved by the overall agreement of experimental and calculated excitation functions. Additionally, particular comments concerning reaction types and residual nuclei follows.

A. ^{nat}Zr$(d,xn)^{97-90}$Nb reactions

1. ^{nat}Zr$(d,n)^{97}$Nb

The measured ^{nat}Zr$(d,n)^{97}$Nb cross sections are for the first time reported in the present work. The analysis of ^{97}Nb

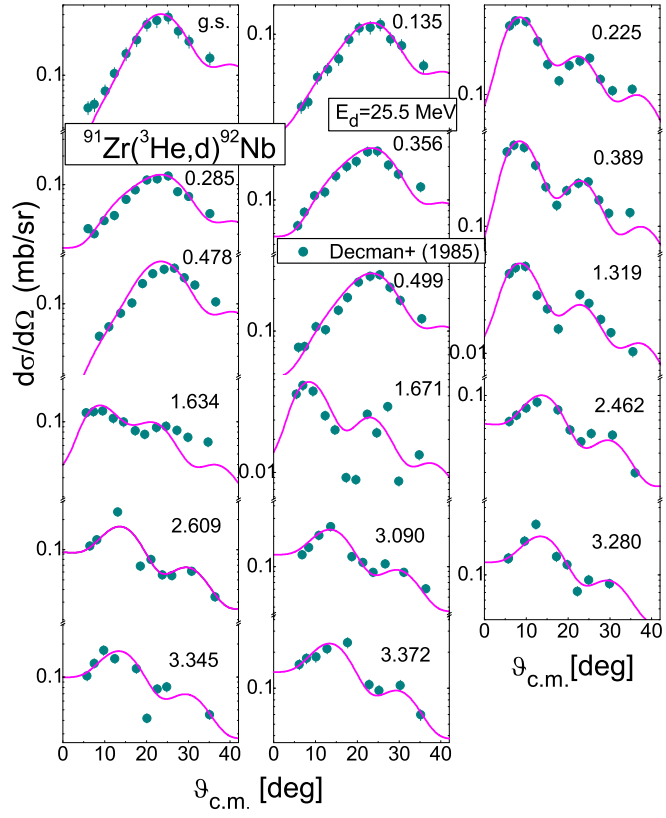

FIG. 9. As in Fig. 8 but for ^{91}Zr$(^3$He$,d)^{92}$Nb reaction at 25.5 MeV [73].

residual-nucleus activation by deuterons incident on ^{nat}Zr target involves actually only the neutron-richest stable isotope ^{96}Zr, while there is an excitation function of the same residual nucleus measured previously for deuterons on the target nucleus ^{96}Zr [85,86].

The suitable description of the ^{97}Nb excitation functions for deuterons incident on ^{nat}Zr as well as ^{96}Zr (Fig. 10) is a distinct test of the present model approach due to the involvement of more reaction mechanisms. However, the

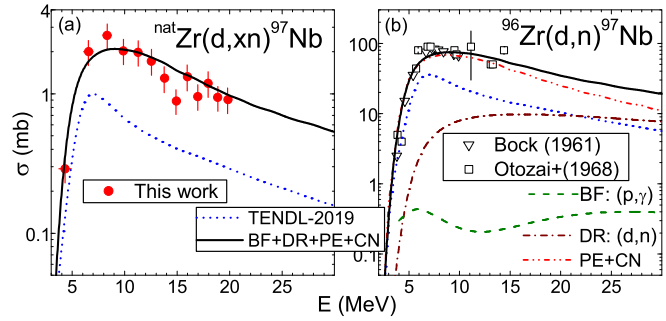

FIG. 10. Comparison of present (solid circles) and previous [85,86] measurements, TENDL-2019 evaluation [22] (short dashed curves), and present calculation (solid curves) of ^{nat}Zr$(d,x)^{97}$Nb and ^{96}Zr$(d,n)^{97}$Nb reaction cross sections, along with BF enhancement (dashed), stripping (d,n) reaction (dash-dotted), and PE + CN components corrected for DI deuteron flux leakage (dash-dot-dotted).

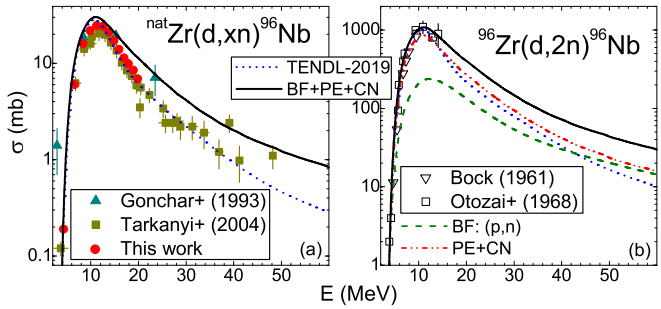

FIG. 11. As in Fig. 10 but for ^{96}Nb activation, and additional data [25,26].

statistical emission has a dominant role in this case, providing a good data account, together with the contribution of the stripping reaction only above the incident energy of ≈15 MeV. The inelastic breakup enhancement brought by breakup protons through the (p,γ) reaction is more than an order of magnitude lower than even the stripping contribution. On the other hand, the apparent underestimation by the TENDL evaluation seems to be due to either different statistical-emission parameters (e.g., the deuteron OMP) or larger BU component.

2. $^{\text{nat}}$Zr$(d,xn)^{96}$Nb

The measured cross sections within the present work are in good agreement particularly with the more recent data [26], while particular support for the higher values around the incident energy of 20 MeV is shown in Fig. 11(a).

The residual nucleus ^{96}Nb population follows actually the deuteron interactions only with the ^{96}Zr isotope, in a similar way to the above-discussed case of ^{97}Nb. That is also because the eventual role of the ^{94}Zr$(d,\gamma)^{96}$Nb reaction is negligible due to the particle/γ decay competition at excitation energies well above particle binding energy. The analysis of the ^{96}Nb activation has taken into account, beyond the PE + CN statistical emission, also the inelastic breakup enhancement brought by breakup protons through the (p,n) reaction, shown in Fig. 11(b). Its weight, of ≈20% around the excitation-function maximum, has led to an accurate account of the measured data for the ^{96}Zr$(d,2n)^{96}$Nb reaction [25,86].

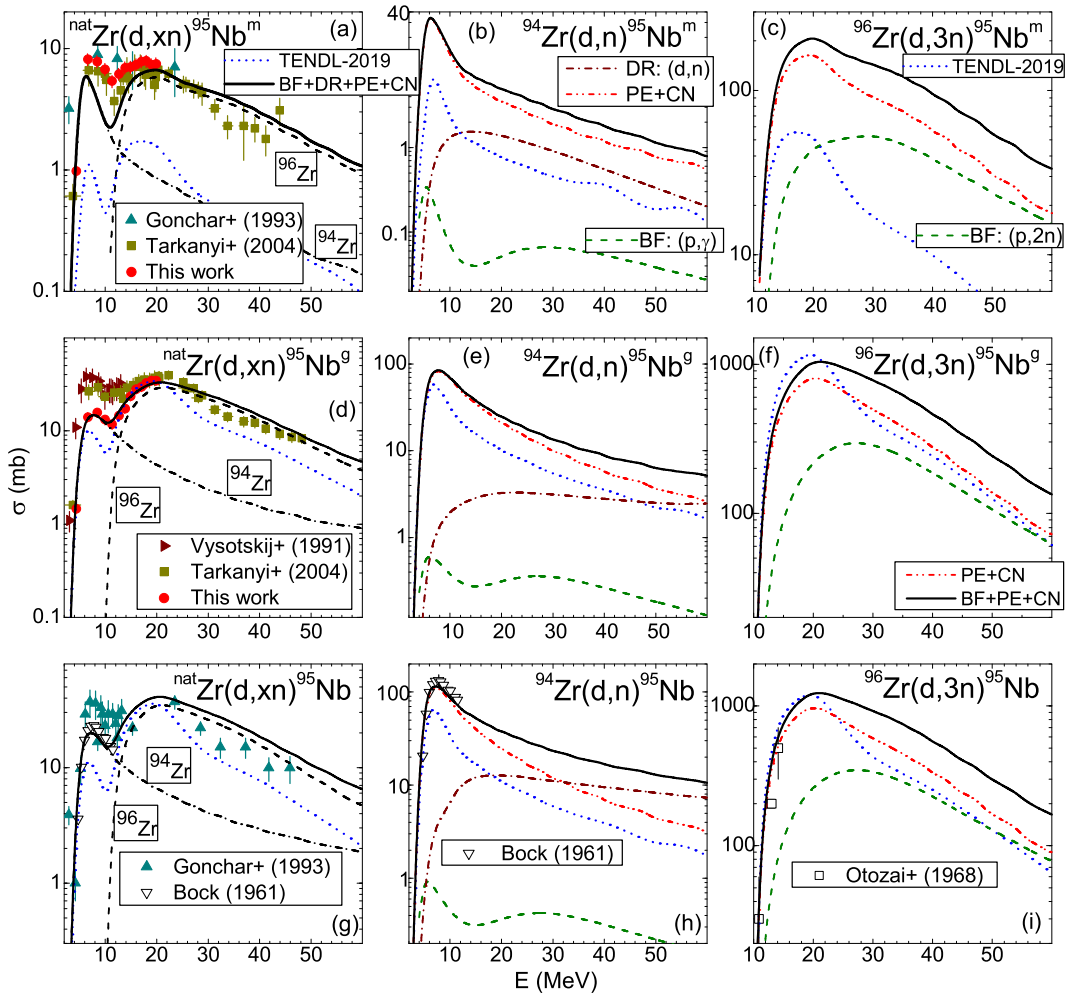

FIG. 12. As in Fig. 11 but for (a)–(c) ^{95}Nb^m, (d)–(f) ^{95}Nb^g, and (g)–(i) ^{95}Nb activation, additional data [40], and (a), (d), (g) ^{94,96}Zr activation contributions (dash-dotted and dashed curves, respectively) (see text).

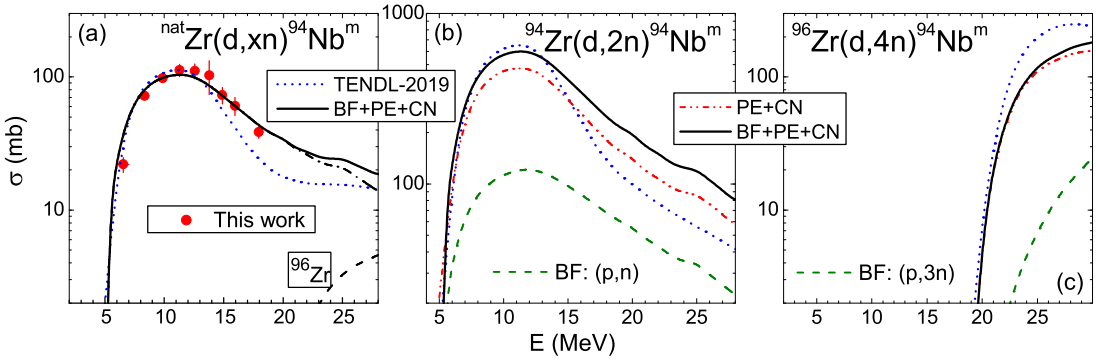

FIG. 13. As in Fig. 12 but for ^{94}Nb^{m} activation.

On the other hand, this BF-enhancement weight increases with energy and provides a less decreasing trend of the corresponding cross sections, but is in agreement with the higher values of the related, rather dispersed data for the $^{\text{nat}}$Zr$(d, xn)^{96}$Nb reaction. Further cross-section measurement in between 20 and 40 MeV within the Neutrons for Science (NFS) project [12] would be quite useful in this respect.

3. $^{\text{nat}}$Zr$(d, xn)^{95}$Nb$^{m,g,m+g}$

While there is a proper correspondence between $^{\text{nat}}$Zr$(d, xn)^{95}$Nb^{m} cross sections measured previously [25–27] and within this work, the apparent difference among the corresponding data for ^{95}Nb^{g} activation (Fig. 12) has already been noted in Sec. II. Moreover, the target stack included also Mo foils earlier [26]. In this case one should note that the γ line of 765.8 keV may correspond also to the decay of both ^{95}Nb (β^-) and ^{95}Tc (β^+, $T^g_{1/2} \approx 20$ h) [56] activated through $^{\text{nat}}$Mo(d, x) reactions [87].

Concerning the model calculations, we first emphasize the suitable account of the ^{95}Nb^{g} activation reported in this work [Fig. 12(d)]. An agreement with the similar data measured previously should include, particularly around their maximum, the contributions from ^{95}Zr decay as mentioned in Sec. II. There is also a good agreement between the experimental and calculated ^{95}Nb^{m} activations [Fig. 12(a)], except for a data underestimation between incident energies 7–11 MeV that preserves their certain shape. Both $^{\text{nat}}$Zr$(d, x)^{95}$Nb and ^{94}Zr$(d, n)^{95}$Nb excitation functions measured by Bock [85] are well described [Figs. 12(g) and 12(h)], while the underestimation of the first maximum of Gonchar *et al.* [25] data could be due to contributions of ^{95}Zr decay.

The PE + CN statistical emission brings the dominant contribution to both (d, n) and $(d, 3n)$ reactions, but also the stripping (d, n) mechanism plays an important role in describing the maximum of the ^{94}Zr(d, n) excitation functions [Figs. 12(a), 12(d), 12(g), 12(h)]. At the same time, the BF enhancement by breakup protons through the $(p, 2n)$ reaction brings an important contribution to ^{96}Zr$(d, 3n)$ activation [Figs. 12(c), 12(f), 12(i)], providing the lower decrease shown by the experimental trend for $^{\text{nat}}$Zr [Figs. 12(a), 12(d), 12(g)]. On the other hand, by comparison of this component and BF enhancement through the (p, γ) reaction contribution to (d, n) reaction cross sections [Figs. 12(b), 12(e), 12(h)], it becomes obvious that there is increased BF importance

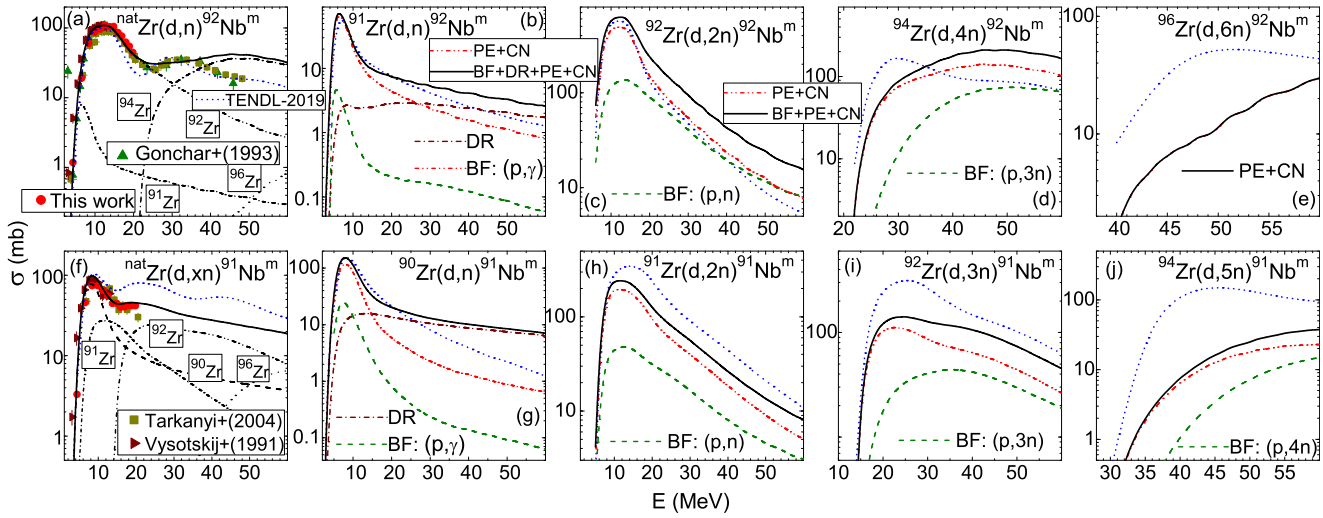

FIG. 14. As in Fig. 12 but for (a)–(e) ^{92}Nb^{m} and (f)–(j) ^{91}Nb^{m} activation, and (a), (f) ^{90,91,92,94,96}Zr activation contributions (dashed, short-dash-dotted, dash-dot-dotted, dash-dotted, and dotted, respectively).

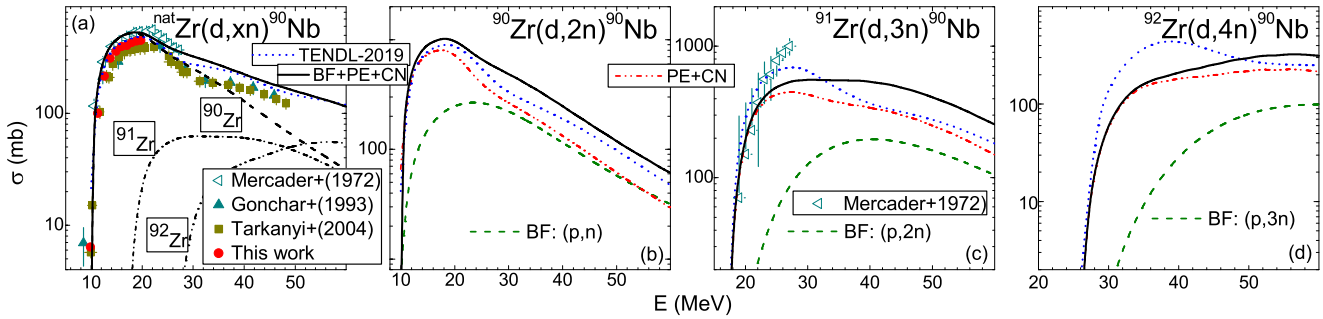

FIG. 15. As in Fig. 14 but for ^{90}Nb activation and additional data [25,26,28,40].

for the third-chance particle emission in deuteron-induced reactions.

Overall, taking into account also the scarce information on branching ratios for ^{95}Nb decay, it may be concluded that a due consideration of BU, DR, and PE + CN processes provides a better account of ^{95}Nb$^{m,g,m+g}$ activation than, e.g., the TENDL-2019 evaluation [Figs. 12(a),12(d),12(g), 12(h)].

4. ^{nat}Zr(d, xn)^{94}Nb^m

The measured ^{nat}Zr(d, xn)^{94}Nb^m excitation function is for the first time reported in the present work, while no other measurement of the corresponding data exists for ^{94,96}Zr target nuclei. This activation is the result of ^{94}Zr(d, $2n$)^{94}Nb^m and ^{96}Zr(d, $4n$)^{94}Nb^m reactions shown in Figs. 13(b) and 13(c), an eventual contribution of the ^{92}Zr isotope through the ^{92}Zr(d, γ)^{94}Nb^m reaction being negligible.

The PE + CN statistical emission provides again the main contribution, while the BF enhancement due to breakup protons through the (p, n) reaction contributes to the description of the ^{nat}Zr(d, xn)^{94}Nb^m excitation-function maximum [Fig. 13(a)]. It has also improved the lower decrease toward the increased incident energies.

5. ^{nat}Zr(d, xn)^{92}Nb^m

The ^{92}Nb^m activation cross sections measured in this work are particularly in agreement with the more recent ones [87] within limits of the error bars. On the other hand, this isomer activation by deuterons on natural Zr includes contributions from ^{91,92,94,96}Zr isotopes and BU, (d, n) stripping, and PE + CN statistical emission mechanisms [Figs. 14(a)–14(e)]. Actually, the dominant ones are due to ^{92,94}Zr isotopes [Fig. 14(a)], following mainly the statistical emission shown in Figs. 14(c) and 14(d). However, important components are also provided by the BF enhancement of breakup protons through (p, n) and (p, $3n$) reactions, respectively [Figs. 14(c) and 14(d)].

Note the related contribution of the less abundant isotope ^{91}Zr, that remains still an order of magnitude lower than that of ^{92,94}Zr isotopes in Fig. 14(a). At the same time, the BF enhancement of breakup protons, through the (p, γ) reaction, is above the stripping ^{91}Zr(d, n)^{92}Nb^m cross sections at incident energies below ≈6 MeV, which then becomes the dominant one at incident energies above 25 MeV [Fig. 14(b)].

Throughout, the present model calculations describe the measured ^{nat}Zr(d, xn)^{92}Nb^m excitation function apart from its decrease at energies beyond ≈40 MeV.

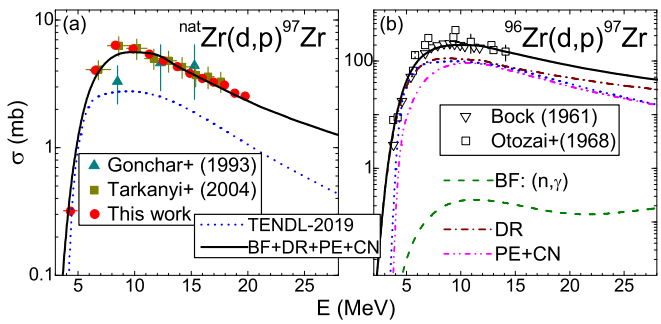

FIG. 16. As in Fig. 10 but for (a) ^{nat}Zr(d, p)^{97}Zr and (b) ^{96}Zr(d, p)^{97}Zr reactions, stripping (d, p) reaction, and previous [25,26,40,85,86] measurements.

6. ^{nat}Zr(d, xn)^{91}Nb^m

The same comments as for ^{92}Nb^m activation are in order for the ^{91}Nb^m isomer, too. The related contributions in this case are due to $^{90–92,94,96}$Zr isotopes, while the main ones are provided by ^{90,91}Zr around the excitation function maximum [Figs. 14(f)–14(j)]. Then, ^{92}Zr becomes more important at energies above 20 MeV. A negligible contribution of the ^{96}Zr(d, $7n$)^{91}Nb^m reaction is no longer shown.

The important role of the DI processes is obvious in Fig. 14(g) above the deuteron energy of 27 MeV, where these reaction mechanisms become dominant. The good agreement between experimental and calculated ^{91}Nb^m activation excitation functions in Fig. 14(f) validates the present model approach.

7. ^{nat}Zr(d, xn)^{90}Nb

The ^{90}Nb activation cross sections measured in this work corroborate the previous lower data sets [25,26], also taking advantage of increased accuracy (Fig. 15).

The description of the ^{nat}Zr(d, xn)^{90}Nb excitation function has taken into account contributions from ^{90,91,92}Zr isotopes, the main one being that of the ^{90}Zr(d, $2n$) reaction [Fig. 15(b)]. The present calculations describe the steep increase of ^{nat}Zr(d, xn)^{90}Nb and ^{91}Zr(d, $3n$)^{90}Nb measured excitation functions [25,26,28] while an overestimation of the former even beyond twice a standard deviation (σ) occurs at deuteron energies above ≈30 MeV [Figs. 15(a)]. It could be a

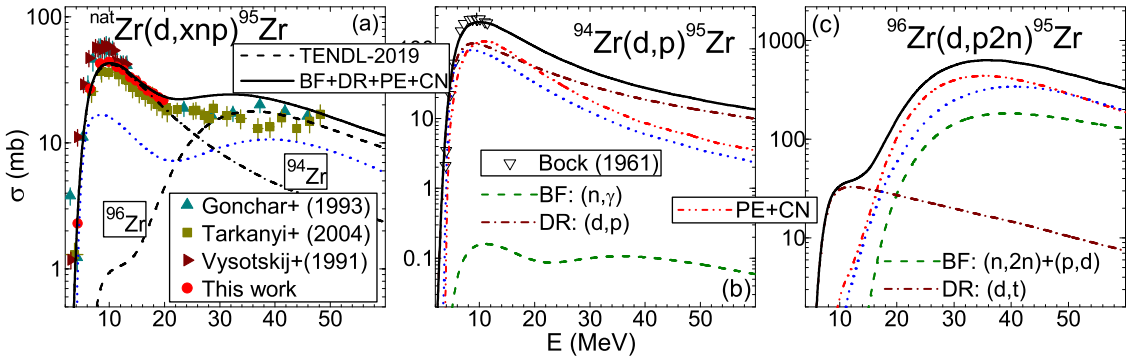

FIG. 17. As in Fig. 12 but for ^{95}Zr activation, additional data [25–27,40,85], and (a) contributions of ^{94}Zr (dash-dotted curve) and ^{96}Zr (dashed curve) isotopes to ^{nat}Zr cross sections.

result of the stronger contribution coming from BF enhancement of breakup protons through the ^{90}Zr$(p,n)^{90}$Nb reaction [Fig. 15(b)] in comparison to the similar ones on ^{92,91}Zr target nuclei [Figs. 14(c) and 14(h)]. At the same time there is also an underestimation of ^{91}Zr$(d,3n)^{90}$Nb measured cross sections above ≈23 MeV, that is slightly improved by the BF enhancement of breakup protons through the ^{91}Zr$(p,2n)^{90}$Nb reaction [Fig. 15(c)].

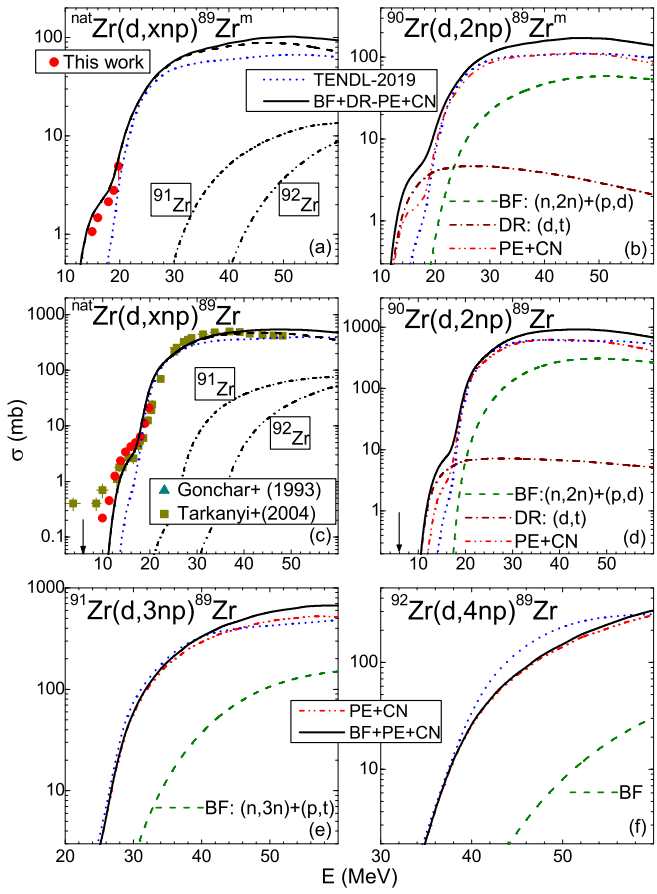

FIG. 18. As in Fig. 14 but for (a), (b) ^{89}Zr^m and and (c)–(f) ^{89}Zr activation, and the additional data [25,26] for the latter; the arrows indicate ^{90}Zr$(d,t)^{89}$Zr reaction threshold.

B. ^{nat}Zr$(d,xnp)^{97-88}$Zr reactions

1. ^{nat}Zr$(d,p)^{97}$Zr

The measured ^{nat}Zr$(d,p)^{97}$Zr cross sections are reported in the present work with much increased accuracy that makes possible the choice of the more recent among two previous data sets at variance [25,26] (Fig. 16). Thus, we clearly established both the maximum of this excitation function and its corresponding deuteron energy.

The analysis of ^{97}Zr residual-nucleus activation by deuterons incident on ^{nat}Zr target involves only the neutron-richest stable isotope ^{96}Zr, in a similar way to the ^{97}Nb activation (Fig. 10). There are also earlier measured cross sections of the same residual nucleus for deuterons incident on the target nucleus ^{96}Zr [85,86].

Once more, similarlty to the (d,n) reaction, description of the latter excitation function in Fig. 16(b) has included the breakup, stripping, and PE + CN statistical emission. However, the BF enhancement by breakup neutrons through the ^{96}Zr$(n,\gamma)^{97}$Zr reaction is two orders of magnitudes lower. On the other hand, the stripping (d,p) process provides now the strongest contribution to ^{97}Zr activation especially at the lowest deuteron energies, below ≈10 MeV, but also above 20 MeV, in good agreement with measured data in Fig. 16.

The effect of neglecting the important role of the DR stripping process is illustrated by the underestimation by the TENDL evaluation of both ^{nat}Zr$(d,p)^{97}$Zr and ^{96}Zr$(d,p)^{97}$Zr reaction data. Actually, this proof is just in line with the previous discussion of the experimental (d,p) excitation functions for ^{51}V [8], ^{50}Cr [7], ^{55}Mn [9], ^{58}Fe [5], ^{59}Co [8], ^{64}Ni [6], and ^{93}Nb [4] target nuclei, which cannot be described as long as the strong stripping (d,p) contribution is neglected.

2. ^{nat}Zr$(d,xnp)^{95}$Zr

The newly measured ^{nat}Zr$(d,xnp)^{95}$Zr cross sections with much increased accuracy are making possible the choice of the more recent data set [26] instead of the earlier ones [25,27], in Fig. 17(a). We have thus clearly established both the maximum of this excitation function and its corresponding deuteron energy.

The analysis of ^{95}Zr residual-nucleus activation through deuteron interaction with natural Zr (Fig. 17) is a most

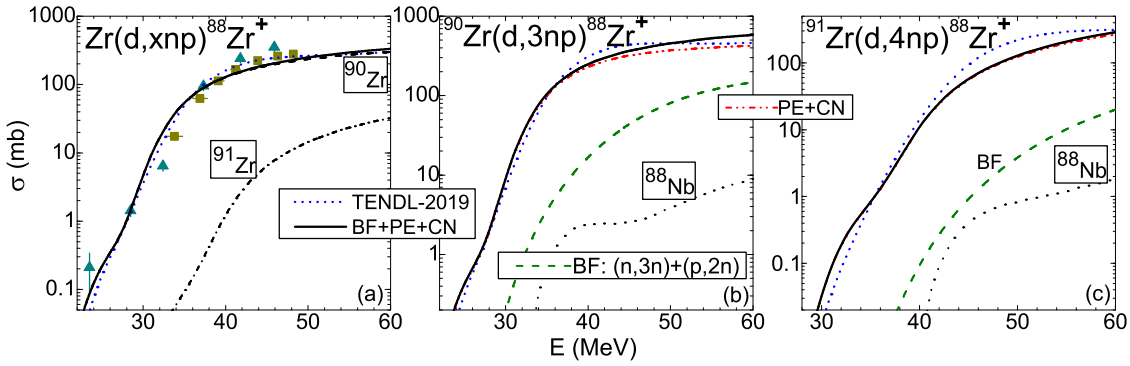

FIG. 19. As in Fig. 14 but for ^{88}Zr cumulative activation including ^{88}Nb residual nucleus decay for (b),(c) deuterons incident on ^{90,91}Zr (dotted curves), and additional data [25,26,40].

interesting one because of the variety of contributing reaction mechanisms. There are involved two direct reactions, namely the stripping ^{94}Zr$(d, p)^{95}$Zr and pickup ^{96}Zr$(d, t)^{95}$Zr reactions, along with the breakup and PE + CN statistical emission [Figs. 17(b) and 17(c)].

The stripping (d, p) mechanism is the dominant one except at deuteron energies between 9 and 20 MeV, where it is close to the statistical PE + CN. Together, they describe well the measured ^{94}Zr$(d, p)^{95}$Zr data [85] [Fig. 17(b)] as well as ^{nat}Zr$(d, xnp)^{95}$Zr excitation functions reported in the present work, providing confidence in the reaction models taken into account. At the same time, the BF enhancement by breakup neutrons through the ^{94}Zr$(n, \gamma)^{95}$Zr reaction is practically negligible.

On the other hand, the pickup (d, t) reaction on the ^{96}Zr isotope provides a contribution much lower above ≈16 MeV than PE + CN and even BF enhancement through $(n, 2n)$ as well as (p, d) reactions on ^{96}Zr [Fig. 17(c)]. However, it is the single reaction mechanism contributing to ^{95}Zr activation below the (d, nd) and $(d, 2np)$ reaction thresholds. This specific feature of the pickup (d, t) process is not apparent in the whole activation of the ^{95}Zr residual nucleus [Fig. 17(a)] due to the strong contribution of the (d, p) reaction at lowest energies. Also note in this respect the large difference between the ^{94,96}Zr isotope weights within natural Zr.

Therefore, ^{95}Zr activation has marked two significant differences between effects of the same reaction mechanism, i.e., major DR stripping (d, p) on ^{94}Zr vs minor pickup (d, t) except at the lowest energies on ^{96}Zr and, on the other hand, major BF enhancement by $(n, 2n)$ and (p, d) reactions on ^{96}Zr vs slight enhancement by the (n, γ) reaction on ^{94}Zr. It proves the need to pay attention to all BU, DR, and PE + CN processes, while the underestimation of the measured ^{95}Zr residual nucleus population by the TENDL evaluation [22] [Figs. 17(a) and 17(b)] could be just due tonot considering the DI.

3. ^{nat}Zr$(d, xnp)^{89}$Zr$^{m,m+g}$

The measured ^{nat}Zr$(d, xnp)^{89}$Zr^{m} excitation function is for the first time reported in the present work, while there are no similar data also for ^{90,91,92}Zr isotopes. At the same time, the newly measured ^{nat}Zr$(d, xnp)^{89}$Zr cross sections are quite helpful in addition to the only previous data set [26] within a large energy range, but showing a less usual behavior below ≈18 MeV (Fig. 18). This behavior is confirmed by the present new data in the limit of 2σ uncertainty, except at the incident energies below 10 MeV, while it is found for the isomer cross section, too. A model analysis becomes thus mandatory for correct insight into this reaction.

Actually it is just the above-discussed (d, t) reaction on ^{90}Zr [Figs. 18(b) and 18(d)] which now gives the full understanding of a break of the two excitation functions' increase within several MeV above the threshold [Figs. 18(a) and 18(c)]. Thus, the pickup reaction ^{90}Zr$(d, t)^{89}$Zr^{m} has

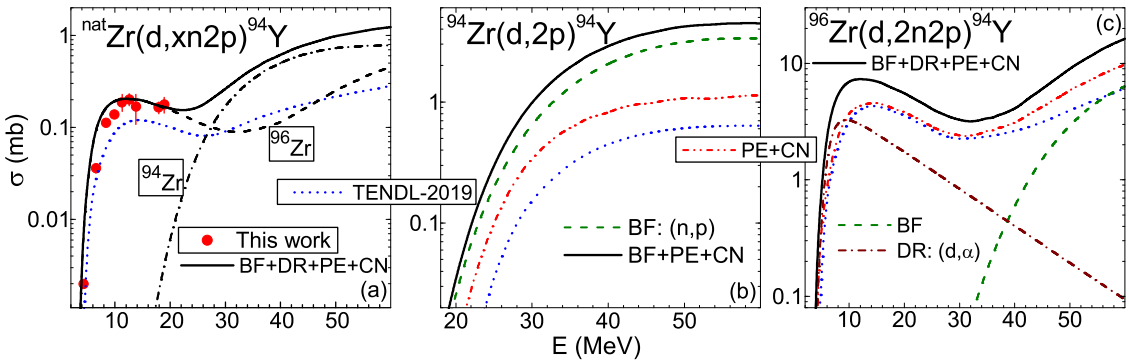

FIG. 20. As in Fig. 12 but for ^{94}Y activation.

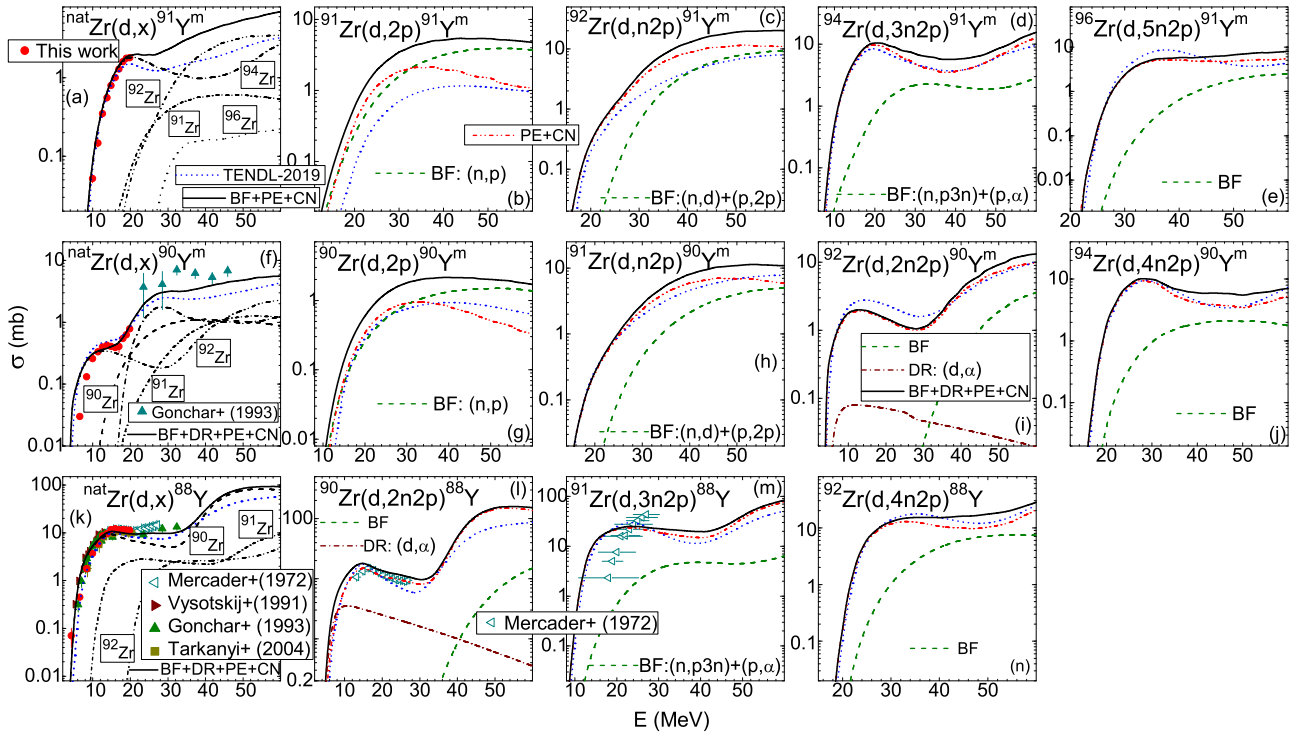

FIG. 21. As in Fig. 14 but for activation of (a)–(e) ^{91}Y^{m}, (f)–(j) ^{90}Y^{m}, and (k)–(n) ^{88}Y.

the major contribution to both excitation functions below 18–20 MeV, while at higher energies it is again much lower than, first, PE + CN and then BF components.

On the other hand, its effect is so much larger in comparison to ^{95}Zr activation due to the major abundance of ^{90}Zr. Consequently, the only PE + CN contributions of the other ^{91,92}Zr isotopes are effective well above either 20 MeV for ^{89}Zr or especially 30 MeV for ^{89}Zr^{m} activation [Figs. 18(a) and 18(c)]. This increased limit for the isomer underlines the usefulness of its present cross-section measurement. Meanwhile, the arrows indicating the ^{90}Zr$(d,t)^{89}$Zr reaction threshold in Figs. 18(c) and 18(d) support the cross sections below 12 MeV measured in this work, at variance with the former data [26] but leading to a better agreement for the presently calculated values. The suitable description of ^{89}Zr activation validates the present DR + BU + PE + CN approach of deuteron interactions, and provides also the grounds of the TENDL [22] underestimation of the low energy range due to lack of due consideration of the pickup (d,t) reaction.

4. $^{\text{nat}}$Zr$(d,xnp)^{88}$Zr

The analysis of ^{88}Zr ($T_{1/2} = 83.4$ d) activation should take into account also the contributing decay of the short-lived ^{88}Nb residual nucleus ($T_{1/2} = 7.78$ min) that makes possible only the measurement of a cumulative population for the former nucleus. The additional activation of ^{88}Nb is shown distinctly for the isotopes ^{90,91}Zr in Figs. 19(b) and 19(c), the contribution of ^{92}Zr to the cross section of the $^{\text{nat}}$Zr$(d,xnp)^{88}$Zr reaction [Fig. 19(a)] being negligible. However, this additional ^{88}Nb activation is obviously much lower than even the BF enhancement by breakup nucleons through, e.g., $(n,3n)$ and $(p,2n)$ reactions in the case of the most abundant isotope ^{90}Zr, which in turn is yet an order of magnitude below the PE + CN component.

Overall, the ^{88}Zr activation by deuterons on $^{\text{nat}}$Zr follows actually the PE + CN statistical $(d,3np)$ reaction on ^{90}Zr. Nevertheless, the good agreement of experimental and calculated excitation functions shown in Fig. 19 proves the whole theoretical framework of the present analysis because the PE + CN component has already been corrected for the DR + BU deuteron-flux decrease.

C. $^{\text{nat}}$Zr$(d,xn2p)^{94-86}$Y reactions

1. $^{\text{nat}}$Zr$(d,xn2p)^{94}$Y

The measured $^{\text{nat}}$Zr$(d,xn2p)^{94}$Y excitation function is reported for the first time in this work, while there are no data also for deuteron-induced reactions on the two heavier ^{94,96}Zr isotopes which contribute to ^{94}Y activation through $(d,2p)$ and $(d,2n2p)$ reactions, respectively. However, its analysis proved really interesting due to less usual DR and BF contributions in addition to the common PE + CN reaction mechanisms.

First, the sharp increase of the pickup (d,α) excitation function on ^{96}Zr in Fig. 20(c), despite being the smallest DR process (Fig. 5), exceeds the PE + CN contribution at incident energies below ≈10 MeV. Actually, it makes the difference between the present calculations and TENDL evaluation that only accounts for the latter process. Then, similar results are provided for a second maximum due to sequential nucleon evaporation above the incident energy of 30 MeV. On the other

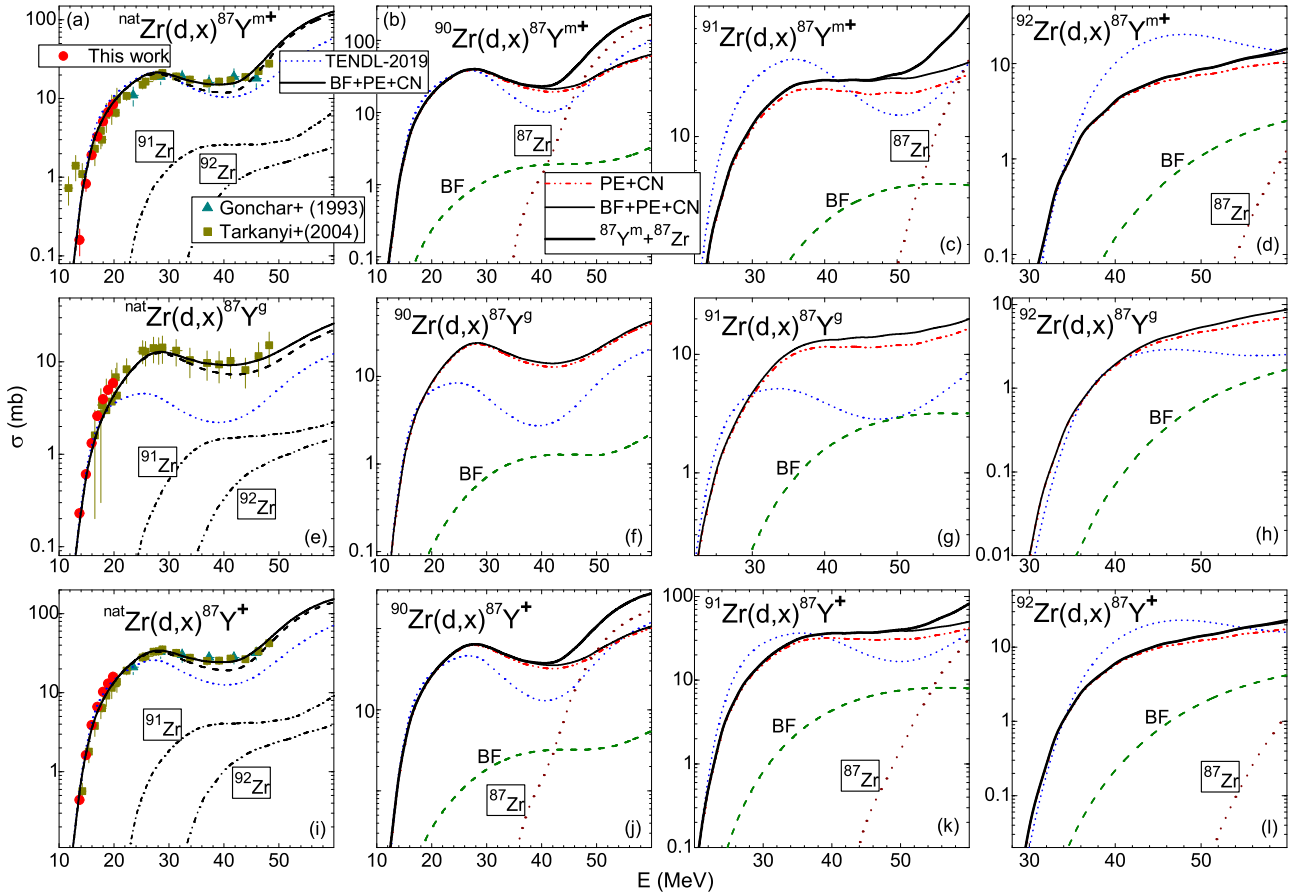

FIG. 22. As in Fig. 14 but for additional data [25,26,40], and (a)–(d) $^{87}Y^{m}$, (e)–(h) $^{87}Y^{g}$, and (i)–(l) ^{87}Y activation as well as (a)–(d),(i)–(l) cumulative population (thick solid) including ^{87}Zr decay (dotted).

hand, even at the higher energies there is an additional component brought by the BF enhancement of breakup nucleons through $^{96}Zr(n, 2np)^{94}Y$ and $^{96}Zr(p, n2p)^{94}Y$ reactions.

Also a BF enhancement due to breakup neutrons through the $^{94}Zr(n, p)^{94}Y$ reaction exceeds by three times the PE + CN component of the reaction $^{94}Zr(d, 2p)^{94}Y$ and rather similar TENDL-2019 predictions [Fig. 20(b)]. This result is essential for the analysis of deuteron interactions with structural materials due to the additional hydrogen accumulation coming mostly from breakup-nucleon-induced reactions.

Lastly, the largest ^{94}Y activation corresponds to the pickup (d, α) reaction on ^{96}Zr below 10 MeV, and BF enhancement through (n, p) reaction on ^{94}Zr above 30 MeV [Fig. 20(a)]. The former component in addition to the corresponding PE + CN provides calculated cross sections in good agreement with the present new data, in support of the actual BF + DR + PE + CN model assessment.

2. $^{nat}Zr(d, xn2p)^{91}Y^{m}$

The $^{nat}Zr(d, xn2p)^{91}Y^{m}$ excitation function has also been measured for the first time in the present work [Fig. 21(a)] while no similar measurement exists for incident deuterons on the stable isotopes $^{91,92,94,96}Zr$. Among them, a contribution to the case of natural Zr at energies of the present measurement can have only $(d, n\alpha)$ reaction on ^{94}Zr, corresponding to the first maximum of the $(d, 3n2p)$ reaction [Fig. 21(d)]. It is given by the PE + CN statistical emission while at the higher energies of the sequential nucleon emission there is a minor addition of the BF enhancement by breakup protons through the (p, α) reaction.

A good account of these data is shown by the present model calculations as well as by TENDL-2019 predictions [Fig. 21(a)]. The latter calculated curve becomes significantly lower above ≈18 MeV due to missing the BF enhancement particularly for the dominant contribution of $(d, n2p)$ on the ^{92}Zr isotope [Fig. 21(c)]. One may also note the contribution of the $^{91}Zr(d, 2p)^{91}Y^{m}$ process [Fig. 21(b)], strongly enhanced by breakup neutrons through the (n, p) reaction in a similar way to the above-discussed case of ^{94}Y activation.

3. $^{nat}Zr(d, xn2p)^{90}Y^{m}$

The $^{nat}Zr(d, xn2p)^{90}Y^{m}$ activation has also been measured for the first time at the lower energies of the present work [Fig. 21(f)] while no other measurement exists for it on the stable isotopes $^{90,91,92,94}Zr$. Contributions of various reactions on these isotopes to $^{90}Y^{m}$ activation are quite similar to the above-discussed $^{91}Y^{m}$, with the difference that now only the (d, α) reaction on ^{92}Zr contributes in the energy range of the $(d, 2n2p)$ reaction first maximum, of the present measurement. A minor addition to the main PE + CN α-particle

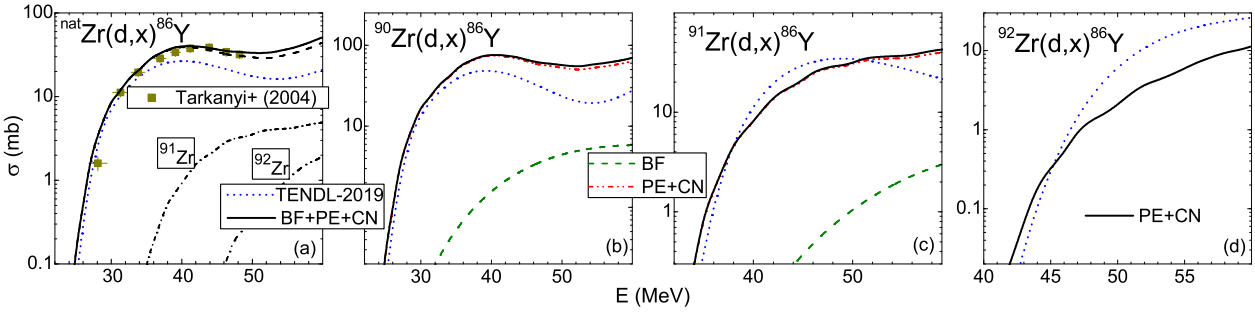

FIG. 23. As in Fig. 15 but for ^{86}Y activation.

statistical emission belongs to the DR pickup reaction mechanism [Fig. 21(i)]. It becomes negligible at the higher energies of the sequential nucleon emission, even in comparison to the BF enhancement by breakup nucleons.

Another similarity with $^{91}Y^m$ activation concerns the $(d, 2p)$ reaction, now on the most abundant isotope ^{90}Zr [Fig. 21(g)]. It is again strongly enhanced by breakup neutrons through the (n, p) reaction pointed out formerly for ^{94}Y and $^{91}Y^m$ activation.

Thus, the final agreement of the newl measured data with presently calculated cross sections is entirely due to the (d, α) reaction on ^{92}Zr, despite its slight role above ≈15 MeV, and also the $(d, 2p)$ reaction on ^{90}Zr above this energy. Contributions of the $(d, 2n\alpha)$ reaction on ^{94}Zr become also important at even higher energies [Fig. 21(j)], before the corresponding sequential nucleon emission, as do contributions of the $(d, n2p)$ reaction on ^{91}Zr [Fig. 21(g)]. The ^{96}Zr isotope contribution is negligible in comparison with the other stable isotopes. The better account of the earlier data [25] at these energies, with reference to TENDL-2019 evaluation, may underline again the importance of the BF enhancement increasing especially the $(d, 2p)$ reaction and thus the hydrogen yield.

On the other hand, the overprediction of the measured cross sections below 10 MeV [Fig. 21(f)] by the (d, α) calculated results may result from (e.g., [84]) an eventual too large α-particle emission corresponding to the OMP [82]. This potential has particularly been used in the present work due to its derivation just for emission of α particles from excited nuclei, while the issue of distinct OMPs for incident and emitted α particles could be resolved in the mass range $A \approx 90$ [84].

4. ^{nat}Zr$(d, xn2p)^{88}$Y

The ^{nat}Zr$(d, xn2p)^{88}$Y activation cross sections measured in the present work, with a really improved accuracy, agree with the previous data within quite larger limits of these data [40] [Fig. 21(k)], while a couple of them extended for two of the three isotopes ^{90,91,92}Zr are able to contribute to ^{nat}Zr activation. The above-mentioned similarity concerning α-particle emission before the corresponding sequential nucleon emission is present in this case, too. However, this ^{88}Y activation follows the (d, α) reaction on the most abundant isotope ^{90}Zr, at the energies of the $(d, 2n2p)$ reaction first maximum as well as of the present measurement [Fig. 21(l)]. Moreover, it is increased by not only the main PE + CN statistical emission but also a DR pickup reaction contribution, becoming negligible at the higher energies even vs the BF enhancement by breakup nucleons [Fig. 21(i)].

There is, too, a contribution of the $(d, n\alpha)$ reaction on ^{91}Zr, at the energies of the $(d, 3n2p)$ reaction first maximum before the corresponding sequential nucleon emission [Fig. 21(m)]. The two different particle-emission sequences are less distinct because of a BF enhancement that reaches a first maximum just in between their top values. The same applies to the $(d, 2n\alpha)$ reaction on ^{92}Zr, at the energies of the $(d, 4n2p)$ reaction first maximum [Fig. 21(n)].

Consequently, the final picture of the ^{88}Y activation for deuterons on ^{nat}Zr has, between 10–20 MeV, not a "shoulder" of 0.5–2 mb but rather a constant value of ≈10 mb up to ≈30 MeV. This trend is fully consistent with the measured cross sections, again except for an overprediction of several data points below the incident energy of 10 MeV. The same cause for this variance of measured and calculated $(d, n\alpha)$ reaction data, with reference to the α-particle OMP [82], could apply. On the other hand, an earlier data set for the $(d, 3n2p)$ reaction on ^{91}Zr has a quite different trend than both present calculation results and the TENDL-2019 evaluation [Fig. 21(m)]. Additional measurement seems necessary.

5. ^{nat}Zr$(d, xn2p)^{87}Y^{m,g,m+g}$

The activation cross sections measured in the present work for the ground state ($\frac{1}{2}^-$, $T_{1/2} = 79.8$ h), isomeric state ($\frac{9}{2}^+$, $T_{1/2} = 13.37$ h), and whole ^{87}Y are in good agreement with the previous data [25,26,40], while their quite improved accuracy provides a better view of these excitation functions especially just above their effective threshold [Figs. 22(a), 22(e), 22(i)]. One may note the missing data for deuterons incident on the ^{90,91,92}Zr isotopes which may contribute to ^{87}Y activation for natural Zr.

The model analysis of ^{90,91,92}Zr contributions to Zr cross sections has shown that PE + CN statistical emission is the dominant process [Figs. 22(b)–22(d), 22(f)–22(h), 22(j)–22(l)]. As for the heavier Y isotopes, the related excitation functions have a first maximum corresponding to the reaction channel $(d, xn\alpha)$ and, following a minimum, a further increase due to the sequential nucleon emission. Despite an obviously lower level, the BF enhancements by breakup nucleons get significant values just at incident energies between these components of $(d, xn\alpha)$ reactions, making less apparent the related minimum.

On the other hand, the most abundant isotope ^{90}Zr has by far the largest contribution to the excitation functions for natural Zr [Figs. 22(a), 22(e), 22(i)]. First, note the good agreement of the presently calculated and measured ^{87}Y activation [Fig. 22(i)], which validates the correctness of the involved model framework. Moreover, the better data agreement above ≈20 MeV, with reference to the TENDL-2019 evaluation, may support particularly the whole present BU approach. At the same time, a similar account of the $^{87}Y^{m,g}$ data has been obtained by using a normalization factor of 0.25 for the spin cutoff parameter of the residual nucleus ^{87}Y [Figs. 22(a) and 22(e)]. Note that this factor value is at variance with, e.g., the value of 0.75 for the spin cutoff parameter of the residual nucleus ^{52}Mn [7]. The two distinct values of this factor correspond not only to different mass ranges but also dissimilar g.s./isomer spins, i.e. $\frac{1}{2}^-$ and $\frac{9}{2}^+$ in the present case vs 2^+ and 6^+ in the latter one. Nevertheless, further moment-of-inertia analysis [83,88–91] as well as new measurements of isomeric-ratio excitation functions would be helpful.

An issue that should be considered, too, is the decay of the residual nucleus ^{87}Zr ($T_{1/2} = 1.68$ h) almost totally to the isomeric state of ^{87}Y [92]. Becauseonly the measurement of a cumulative activation of the isomeric states of $^{87}Y^m$ and ^{87}Y nuclei has been possible, the calculated results corresponding to ^{90,91,92}Zr$(d, xnp)^{87}$Zr have been used for assessment of these cumulative cross sections [Figs. 22(a)–(d) and 22(i)–(l)]. Activation of ^{87}Zr following sequential emission of also five nucleons, with one neutron replacing a proton but no clusterization effect, becomes even

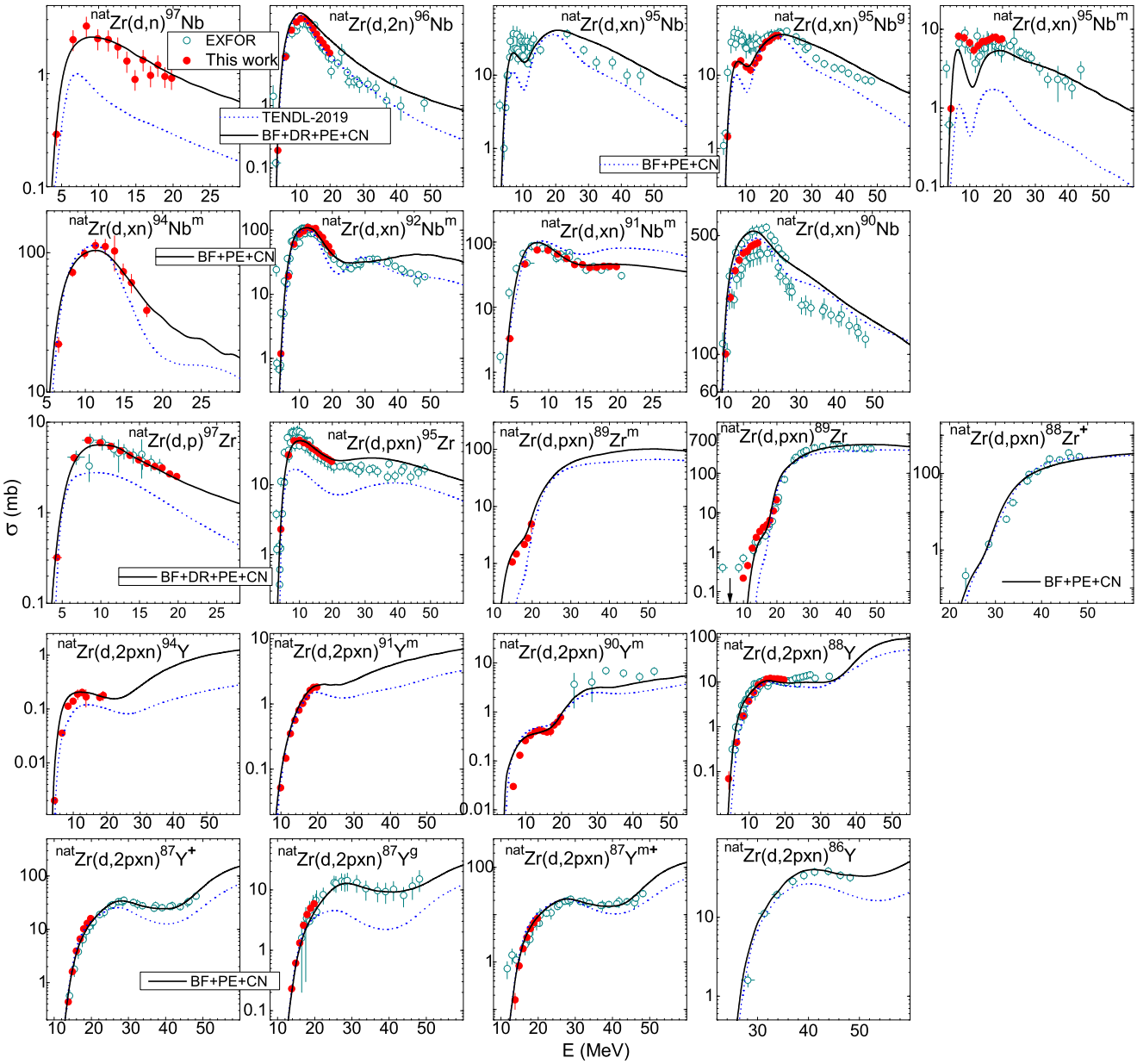

FIG. 24. Comparison of previous [25–28,40,85,86] (open circles) and present (solid circles) measurements, TENDL-2019 evaluation [22] (short dashed curves), and present calculations (solid curves) of the activation cross sections of deuteron-induced reactions on ^{nat}Zr.

larger than the straight one of ^{87}Y above an incident energy of ≈47 MeV. Therefore, conclusions of the present comparison with the data available below this energy remain unchanged.

6. ^{nat}Zr(d, $xn2p$)^{86}Y

Every comment concerning ^{87}Y activation applies equally well to the case of ^{86}Y except for an excitation functions shift to higher energies, related to emission of an additional neutron, and no cumulative effect (Fig. 23).

Finally, it is noteworthy that discussion of $(d, xn2p)$ reactions concerns a most important issue of the nuclear engineering design of international projects such as ITER [10] and DEMO [17], namely the H and He gas accumulation in their structural materials. Its correct assessment demands a thoroughgoing consideration of both deuteron and breakup-nucleon-induced reactions, experimentally as well as by consistent model analysis.

V. CONCLUSIONS

The activation cross sections for production of ^{90,91m,92m,94m,95m,95g,96,97}Nb, ^{89m,89,95,97}Zr, and ^{87m,87g,87,88,90m,91m,94}Y nuclei in deuteron-induced reactions on natural Zr were measured at deuteron energies up to 20 MeV. The ^{nat}Zr$(d, x)^{94m,97}$Nb, ^{nat}Zr$(d, x)^{89m}$Zr, and ^{nat}Zr$(d, x)^{91m,94}$Y excitation functions have been measured for the first time, enriching the deuteron database as strongly requested by large-scale research projects [10–12]. Moreover, the new measurements have been quite useful for validation of direct interactions modeling, stressing their role in description of the deuteron-induced reactions. The other measured data reported in the present work support furthermore the previous data [25–28,40,85,86] but with much increased accuracy.

The whole systematics of the activation data within deuteron-induced reactions on ^{nat}Zr, at incident energies up to 60 MeV, is summarized in Fig. 24 and compared with TENDL-2019 evaluation [22] and the model calculations carried out within present work. Each excitation function has been described through a unitary and consistent analysis of all reaction mechanisms involved in the complex deuteron interaction process, e.g., elastic scattering, breakup, stripping, pickup, preequilibrium, and compound nucleus. The detailed theoretical treatment of each reaction mechanism has thus been proved necessary to obtain a reliable understanding of the interaction process as well as accurate values of calculated deuteron activation cross sections.

The theoretical framework has been supported by comparison of the experimental data with the present calculations as well as the corresponding TENDL-2019 evaluation [22]. Distinct discrepancies can be obviously related to the complexity of the interaction process, not entirely accounted for in routine evaluation/theoretical analyses. As shown in Sec. IV, most of them are due to overlooking the deuteron inelastic-breakup enhancement and appropriate treatment of stripping and pickup processes. This comparative analysis of experimental data, evaluations, and model calculations stresses the weak points and consequently the need for theoretical framework/evaluation upgrade, as well as requirements for new measurements.

The consistent theoretical approach to the deuteron interactions, supported by advanced codes associated with the nuclear reaction mechanisms, provides not only the description of data, but especially predictability. While actual applications have yet to involve deuteron-data fit, e.g., by various-order genuine Padé approximations for high-priority elements [18,19,50], the related predictive power remains low. Conversely, update of the theoretical framework of deuteron-nucleus interaction will improve the evaluation predictions for target nuclei and incident energies where data are still missing, but strongly requested by engineering design projects [10–12].

However, increased attention should be paid to theoretical description of the breakup mechanism, including its inelastic component, in order to bring it to the level of the current theoretical models for stripping, pickup, preequilibrium emission, and compound-nucleus mechanisms. The continuous interest in the breakup theoretical analysis, e.g., [93–97], could provide improved deuteron-breakup empirical parametrization and, thus, more accurate activation cross sections. On the other hand, this improvement requires, first, an overall increase of the deuteron-data basis energy range to ≈40 MeV [12] and, second, also complementary measurements of (d, px) and (n, x) as well as (d, nx) and (p, x) reaction cross sections for the same target nucleus, within corresponding incident-energy ranges.

ACKNOWLEDGMENTS

This work has been partly supported by OP RDE, MEYS, Czech Republic under the project SPIRAL2-CZ, CZ.02.1.01/0.0/0.016_013/0001679, and by Autoritatea Nationala pentru Cercetare Stiintifica (Project PN-19060102).

[1] P. Bém, E. Šimečková, M. Honusek, U. Fischer, S. P. Simakov, R. A. Forrest, M. Avrigeanu, A. C. Obreja, F. L. Roman, and V. Avrigeanu, Phys. Rev. C **79**, 044610 (2009).

[2] E. Šimečková, P. Bém, M. Honusek, M. Štefánik, U. Fischer, S. P. Simakov, R. A. Forrest, A. J. Koning, J.-C. Sublet, M. Avrigeanu, F. L. Roman, and V. Avrigeanu, Phys. Rev. C **84**, 014605 (2011); I. Mardor, M. Avrigeanu, D. Berkovits, A. Dahan, T. Dickel, I. Eliyahu, S. Halfon, M. Hass, T. Hirsh, D. Kijel *et al.*, Eur. Phys. J. A **54**, 91 (2018).

[3] M. Avrigeanu, V. Avrigeanu, and A. J. Koning, Phys. Rev. C **85**, 034603 (2012).

[4] M. Avrigeanu, V. Avrigeanu, P. Bém, U. Fischer, M. Honusek, A. J. Koning, J. Mrázek, E. Šimečková, M. Štefánik, and L. Zaváorka, Phys. Rev. C **88**, 014612 (2013).

[5] M. Avrigeanu, V. Avrigeanu, P. Bém, U. Fischer, M. Honusek, K. Katovsky, C. Mănăilescu, J. Mrázek, E. Šimečková, and L. Zaváorka, Phys. Rev. C **89**, 044613 (2014); M. Avrigeanu and V. Avrigeanu, Nucl. Data Sheets **118**, 301 (2014).

[6] M. Avrigeanu, E. Šimečková, U. Fischer, J. Mrázek, J. Novak, M. Štefánik, C. Costache, and V. Avrigeanu, Phys. Rev. C **94**, 014606 (2016).

[7] E. Šimečková, M. Avrigeanu, U. Fischer, J. Mrázek, J. Novak, M. Štefánik, C. Costache, and V. Avrigeanu, Phys. Rev. C **98**, 034606 (2018).

[8] A. Kreisel, L. Weissman, A. Cohen, T. Hirsh, A. Shor, O. Aviv, I. Eliyahu, M. Avrigeanu, and V. Avrigeanu, Phys. Rev. C **99**, 034611 (2019).

[9] M. Avrigeanu, E. Šimečková, U. Fischer, J. Mrázek, J. Novak, M. Štefánik, C. Costache, and V. Avrigeanu, Phys. Rev. C **101**, 024605 (2020).

[10] https://www.iter.org/

[11] http://www.ifmif.org/.

[12] X. Ledoux *et al.*, Radiat. Prot. Dosim. **180**, 115 (2018); Eur. Phys. J. A **57**, 257 (2021), https://www.ganil-spiral2.eu/scientists/ganil-spiral-2-facilities/experimental-areas/nfs/.

[13] M. Avrigeanu, W. von Oertzen, R. A. Forrest, A. C. Obreja, F. L. Roman, and V. Avrigeanu, Fusion Eng. Des. **84**, 418 (2009).

[14] M. Avrigeanu and A. M. Moro, Phys. Rev. C **82**, 037601 (2010).

[15] M. Avrigeanu and V. Avrigeanu, Phys. Rev. C **95**, 024607 (2017).

[16] Fusion Evaluated Nuclear Data Library (FENDL) 3.0, https://www-nds.iaea.org/fendl30/

[17] F. Mota, I. Palermo, S. Laces, J. Molla, and A. Ibarra, Nucl. Fusion **57**, 126056 (2017).

[18] A. Hermanne, A. V. Ignatyuk, R. Capote, B. V. Carlson, J. W. Engle, M. A. Kellett, T. Kibédi, G. Kim, F. G. Kondev, M. Hussain *et al.*, Nucl. Data Sheets **148**, 338 (2018).

[19] J. W. Engle, A. V. Ignatyuk, R. Capote, B. V. Carlson, A. Hermanne, M. A. Kellett, T. Kibédi, G. Kim, F. G. Kondev, M. Hussain *et al.*, Nucl. Data Sheets **155**, 56 (2019).

[20] I. J. Thompson, Comput. Phys. Rep. **7**, 167 (1988); FRESCO v. 2.9, 2011, LLNL-SM-485670, http://www.fresco.org.uk/input2.9/html/index.html

[21] A. J. Koning, S. Hilaire, and M. C. Duijvestijn, TALYS-1.0, in *Proceedings of the International Conference on Nuclear Data for Science and Technology*, April 22–27, 2007, Nice, France, edited by O. Bersillon, F. Gunsing, E. Bauge, R. Jacqmin, and S. Leray (EDP Sciences, Paris, 2008), p. 211; v. TALYS-1.95, 2019, http://www.talys.eu.

[22] A. J. Koning and D. Rochman, Nucl. Data Sheets **113**, 2841 (2012); A. J. Koning *et al.*, TENDL-2019: TALYS-based evaluated nuclear data library, https://tendl.web.psi.ch/tendl_2019/tendl2019.html

[23] J. F. Ziegler, J. P. Biersack, and M. D. Ziegler, SRIM, The Stopping and Range of Ions in Matter, computer code, http://www.srim.org.

[24] S. Y. F. Chu, L. P. Ekström, and R. B. Firestone, The Lund/LBNL Nuclear Data, Search Version 2.0, February 1999, http://nucleardata.nuclear.lu.se/toi/.

[25] A. V. Gonchar, S. N. Kondratyev, Ju. N. Lobach, S. V. Nevskij, V. D. Skljarenko, and V. V. Tokarevskij, EXFOR database, file EXFOR A0565 dated May 22, 1996, https://www-nds.iaea.org/exfor/.

[26] F. Tarkanyi, A. Hermanne, S. Takacs, F. Ditroi, A. I. Dityuk, and Yu. N. Shubin, Nucl. Instrum. Methods Phys. Res. B **217**, 373 (2004).

[27] O. N. Vysotskij, A. V. Gonchar, O. K. Gorpinich, S. N. Kondrat, V. S. Prokopenko, S. B. Rakitin, V. D. Skljarenko, and V. V. Tokarevskij, EXFOR database, file EXFOR O0380 dated June 19, 1997.

[28] R. C. Mercader, M. C. Caracoche, and A. B. Mocoroa, Z. fur Physik **255**, 103 (1972).

[29] N. M. Anton'eva, A. V. Barkov, A. V. Zolotavin, G. S. Katykhin, V. M. Makarov, and V. O. Sergeev, Izv. Akad. Nauk SSSR Ser. Fiz. **38**, 1741 (1974).

[30] W. W. Daehnick, J. D. Childs, and Z. Vrcelj, Phys. Rev. C **21**, 2253 (1980).

[31] L. D. Knutson and W. Haeberli, Phys. Rev. C **12**, 1469 (1975).

[32] J. M. Lohr and W. Haeberli, Nucl. Phys. A **232**, 381 (1974).

[33] H. R. Burgi, W. Gruebler, J. Nurzynski, V. Konig, P. A. Schmelzbach, R. Risler, B. Jenny, and R. A. Hardekopf, Nucl. Phys. A **321**, 445 (1979).

[34] R. P. Goddard and W. Haeberli, Nucl. Phys. A **316**, 116 (1979).

[35] R. D. Rathmell, P. J. Bjorkholm, and W. Haeberli, Nucl. Phys. A **206**, 459 (1973).

[36] M. Ermer, H. Clement, G. Holetzke, W. Kabitzke, G. Graw, R. Hertenberger, H. Kader, F. Merz, and P. Schiemenz, Nucl. Phys. A **533**, 71 (1991).

[37] R. Roche, N. Van Sen, G. Perrin, J. C. Gondrand, A. Fiore, and H. Muller, Nucl. Phys. A **220**, 381 (1974).

[38] N. Matsuoka, H. Sakai, T. Saito, K. Hosono, M. Kondo, H. Ito, K. Hatanaka, T. Ichihara, A. Okihana, K. Imai, and K. Nisimura, Nucl. Phys. A **455**, 413 (1986).

[39] E. Newman, L. C. Becker, and B. M. Freedom, Nucl. Phys. A **100**, 225 (1967).

[40] N. Otuka *et al.*, Nucl. Data Sheets **120**, 272 (2014); V. V. Zerkin and B. Pritychenko, Nucl. Instrum. Methods Phys. Res. A **888**, 31 (2018); Experimental Nuclear Reaction Data (EXFOR), https://www-nds.iaea.org/exfor/

[41] O. Bersillon, Code SCAT2, CEA Technical Report No. CEA-N-2227, CEN, Bruyéres-le-Châtel, 1981, http://www.oecd-nea.org/tools/abstract/detail/nea-0829/.

[42] J. Pampus, J. Bisplinghoff, J. Ernst, T. Mayer-Kuckuk, J. Rama Rao, G. Baur, F. Rosel, and D. Trautmann, Nucl. Phys. A **311**, 141 (1978).

[43] J. R. Wu, C. C. Chang, and H. D. Holmgren, Phys. Rev. C **19**, 370 (1979).

[44] J. Kleinfeller, J. Bisplinghoff, J. Ernst, T. Mayer-Kuckuk, G. Baur, B. Hoffmann, R. Shyam, F. Rosel, and D. Trautmann, Nucl. Phys. A **370**, 205 (1981).

[45] N. Matsuoka, M. Kondo, A. Shimizu, T. Saito, S. Nagamachi, H. Sakaguchi, A. Goto, and F. Ohtani, Nucl. Phys. A **345**, 1 (1980).

[46] M. G. Mustafa, T. Tamura, and T. Udagawa, Phys. Rev. C **35**, 2077 (1987).

[47] M. Avrigeanu, V. Avrigeanu, and C. Costache, EPJ Web Conf. **146**, 12020 (2017); M. Avrigeanu, C. Costache, and V. Avrigeanu, *ibid.* **239**, 03011 (2020); M. Avrigeanu and V. Avrigeanu, *Proceedings of the 15th International Conference on Nuclear Reaction Mechanisms*, Varenna, Italy, 2018, edited by F. Cerutti *et al.*, CERN Proceedings 2019-001 (CERN, Geneva, 2019), pp. 131; M. Avrigeanu and V. Avrigeanu, J. Phys: Conf. Ser. **724**, 012003 (2016); **1023**, 012009 (2018); in *Exotic Nuclei and Nuclear/Particle Astrophysics (VII). Physics with Small Accelerators: Proceedings of the Carpathian Summer School of Physics 2018 (CSSP18)*, 1–14 July 2018, Sinaia, Romania, AIP Conf. Proc. No. 2076 (AIP, New York, 2019), p. 020003.

[48] M. Avrigeanu, V. Avrigeanu, and C. Manailescu, in *Exotic Nuclei and Nuclear/Particle Astrophysics (V). From Nuclei to Stars: Carpathian Summer School of Physics 2014*, 13–26 July 2014, Sinaia, Romania, edited by L. Trache, D. Chesneanu, and C. A. Ur, AIP Conf. Proc. No. 1645 (AIP, New York, 2015),

p. 139; M. Avrigeanu and V. Avrigeanu, EPJ Web Conf. **2**, 01004 (2010); **21**, 07003 (2012); J. Phys: Conf. Ser. **205**, 012014 (2010); **533**, 012004 (2014); **1555**, 0122016 (2020); J. Korean Phys. Soc. **59**, 903 (2011).
[49] M. Avrigeanu and V. Avrigeanu, Phys. Rev. C **92**, 021601(R) (2015).
[50] F. Tarkányi, A. Hermanne, F. Ditrói, S. Takács, A. V. Ignatyuk, I. Spahan, and S. Spellerberg, Eur. Phys. J. A **57**, 21 (2021).
[51] Y. Iseri, M. Yahiro, and M. Kamimura, Prog. Theor. Phys. Suppl. **89**, 84 (1986).
[52] P. Guazzoni, L. Zetta, A. Covello, A. Gargano, B. F. Bayman, T. Faestermann, G. Graw, R. Hertenberger, H.-F. Wirth, and M. Jaskola, Phys. Rev. C **83**, 044614 (2011).
[53] R. M. DelVecchio, Phys. Rev. C **7**, 677 (1973).
[54] Evaluated Nuclear Structure Data File (ENSDF), http://www.nndc.bnl.gov/ensdf/.
[55] C. M. Baglin, Nucl. Data Sheets **114**, 1293 (2013); **113**, 2187 (2012); **112**, 1163 (2011).
[56] S. K. Basu, G. Mukherjee, and A. A. Sonzogni, Nucl. Data Sheets **111**, 2555 (2010).
[57] N. Nica, Nucl. Data Sheets **111**, 525 (2010).
[58] E. Browne, Nucl. Data Sheets **82**, 379 (1997).
[59] D. Abriola and A. A. Sonzogni, Nucl. Data Sheets **107**, 2423 (2006).
[60] E. A. Mccutchan and A. A. Sonzogni, Nucl. Data Sheets **115**, 135 (2014).
[61] B. Singh, Nucl. Data Sheets **114**, 1 (2013).
[62] H. P. Block, L. Hulstman, E. J. Kaptein, and J. Blok, Nucl. Phys. A **273**, 142 (1976).
[63] T. Borello-Lewin, H. M. A. Castro, L. B. Horodynski-Matsushigue, and O. Dietzsch, Phys. Rev. C **20**, 2101 (1979).
[64] H. Fann and U. Strohbuschf, Phys. Rev. C **6**, 2299 (1972).
[65] C. H. Bingham and G. T. Fabian, Phys. Rev. C **7**, 1509 (1973).
[66] J. L. Horton, C. L. Hollas, P. J. Riley, S. A. A. Zaidi, C. M. Jones, and J. L. C. Ford, Jr., Nucl. Phys. A **190**, 362 (1972).
[67] W. W. Daehnick and T. S. Bhatia, Phys. Rev. C **7**, 2366 (1973).
[68] Shigeru Takeda, J. Phys. Soc. Jap. **34**, 304 (1973).
[69] R. Jahr and R. Santo, Nucl. Phys. **67**, 401 (1965).
[70] K. Suzuki, J. Kawa, and K. Okada, Nucl. Phys. A **228**, 513 (1974).
[71] S. Gilad, S. Cochavi, M. A. Moinester, J. Alster, M. Buenerd, and P. Martin, Nucl. Phys. A **233**, 81 (1974).
[72] I. R. Medsker and J. L. Yntema, Phys. Rev. C **7**, 440 (1973).
[73] D. J. Decman and R. K. Sheline, Z. Phys. A **322**, 37 (1985).
[74] D. M. Janseitov, S. M. Lukyanov, K. Mendibayev, Yu. E. Penionzhkevich, N. K. Skobelev, Yu. G. Sobolev, K. A. Kuterbekov, D. S. Valiolda, T. K. Zholdybayev, L. N. Gumilyov *et al.*, Int. J. Mod. Phys. E **27**, 1850089 (2018).
[75] See Supplemental Material at http://link.aps.org/supplemental/10.1103/PhysRevC.104.044615 for the spectroscopic factors obtained in the present work by analysis of experimental outgoing-particle angular distributions.
[76] N. K. Timofeyuk and R. C. Johnson, Prog. Part. Nucl. Phys. **111**, 103738 (2020).
[77] D. Walter, S. D. Pain, J. A. Cizewski, F. M. Nunes, S. Ahn, T. Baugher, D. W. Bardayan, T. Baumann, D. Bazin, S. Burcher, K. A. Chipps, G. Cerizza, K. L. Jones, R. L. Kozub, S. J. Lonsdale, B. Manning, F. Montes, P. D. O'Malley, S. Ota, J. Pereira, A. Ratkiewicz *et al.*, Phys. Rev. C **99**, 054625 (2019).
[78] M. B. Tsang, Jenny Lee, S. C. Su, J. Y. Dai, M. Horoi, H. Liu, W. G. Lynch, and S. Warren, Phys. Rev. Lett. **102**, 062501 (2009).
[79] Shubhchintak and P. Descouvemont, Phys. Lett. B **811**, 103738 (2020).
[80] A. J. Koning and J. P. Delaroche, Nucl. Phys. A **713**, 231 (2003).
[81] F. D. Becchetti, Jr. and G. W. Greenlees, *John H. Wiliams Laboratory Annual Report 1969* (Minnesota University, Minneapolis, 1969), p. 116.
[82] V. Avrigeanu, P. E. Hodgson, and M. Avrigeanu, Phys. Rev. C **49**, 2136 (1994).
[83] P. Reimer, V. Avrigeanu, S. V. Chuvaev, A. A. Filatenkov, T. Glodariu, A. Koning, A. J. M. Plompen, S. M. Qaim, D. L. Smith, and H. Weigmann, Phys. Rev. C **71**, 044617 (2005).
[84] V. Avrigeanu and M. Avrigeanu, Phys. Rev. C **96**, 044610 (2017).
[85] R. Bock, Z. Phys. **164**, 546 (1961).
[86] K. Otozai, S. Kuze, H. Okamura, A. Mito, T. Nishi, and I. Fujiwara, Nucl. Phys. A **107**, 427 (1968).
[87] F. Tarkanyi, F. Ditroi, S. Takacs, B. Kiraly, A. Hermanne, M. Sonck, M. Baba, and A. V. Ignatyuk, Nucl. Instrum. Methods Phys. Res. B **274**, 1 (2012).
[88] V. Avrigeanu, T. Glodariu, A. J. M. Plompen, and H. Weigmann, J. Nucl. Sci. Technol. **39**, 746 (2002).
[89] V. Semkova, V. Avrigeanu, T. Glodariu, A. J. Koning, A. J. M. Plompen, D. L. Smith, and S. Sudar, Nucl. Phys. A **730**, 255 (2004).
[90] V. Avrigeanu, R. Eichin, R. A. Forrest, H. Freiesleben, M. Herman, A. J. Koning, and K. Seidel, Nucl. Phys. A **765**, 1 (2006).
[91] M. Avrigeanu S. Chuvaev, A. A. Filatenko, R. A. Forrest, M. Herman, A. J. Koning, A. J. M. Plompen, F. L. Roman, and V. Avrigeanu, Nucl. Phys. A **806**, 15 (2008).
[92] T. D. Johnson and W. D. Kulpa, Nucl. Data Sheets **129**, 1 (2015).
[93] Y. S. Neoh, K. Yoshida, K. Minomo, and K. Ogata, Phys. Rev. C **94**, 044619 (2016).
[94] B. V. Carlson, R. Capote, and M. Sin, Few-Body Syst. **57**, 307 (2016).
[95] K. Ogata and K. Yoshida, Phys. Rev. C **94**, 051603(R) (2016).
[96] G. Potel, F. M. Nunes, and I. J. Thompson, Phys. Rev. C **92**, 034611 (2015).
[97] Jin Lei and A. M. Moro, Phys. Rev. C **92**, 044616 (2015).